J. Fluid Mech. (1994), *vol.* 267, *pp.* 153–183

A new vectorial bedload formulation and its application to the time evolution of straight river channels

By AGNES KOVACS† AND GARY PARKER

St Anthony Falls Hydraulic Laboratory, Department of Civil and Mineral Engineering, University of Minnesota, Mississippi River at 3rd Avenue SE, Minneapolis, MN 55414, USA

(Received 27 March 1992 and in revised form 14 September 1993)

The derivation of a new vectorial bedload formulation for the transport of coarse sediment by fluid flow is presented in the first part of the paper. This relation has been developed for slopes up to the angle of repose both in the streamwise and transverse directions. The pressure distribution is assumed to be hydrostatic. The bed shear stress for the onset of particle motion and mean particle velocity are obtained from the mean force balance on a particle. A new generalized Bagnold hypothesis is introduced to calculate the sediment content of the bedload layer. The new formulation possesses two innovative features. It is fully nonlinear and vectorial in nature, in addition, it behaves smoothly up to the angle of repose.

A mathematical model of the time evolution of straight river channels is presented in the second half of the paper. This study focuses on the evolution process due to bank erosion in the presence of bedload only. The bed and bank material is taken to be coarse, non-cohesive and uniform in size. The sediment continuity and the fluid momentum conservation equations describe the time evolution of the bed topography and flow field. These equations are coupled through the fluid shear stress acting on the bed. This bed shear stress distribution is predicted with the aid of a simple algebraic turbulent closure model. As regards the computation of the sediment flux, the new fully nonlinear vectorial formulation is found to perform well and renders the evolution model fully mechanistic.

The formation of an erosional front in the time development of straight river channels has been so far obscured in physical experiments. Herein, with the help of the new bedload formulation, the existence and migration speed of the front of erosion are inferred from the analysis of the sediment continuity equation.

The model successfully describes the time relaxation of an initially trapezoidal channel toward an equilibrium cross-sectional shape, as evidenced by comparison with experimental data. This equilibrium is characterized by a constant width, vanishing sediment transport in the transverse direction, and a small but non-vanishing streamwise transport rate of bed sediment.

1. Introduction

Under certain conditions the interaction of the flow and non-cohesive bed material results in the motion of sediment particles. Depending on the magnitude of the shear stress exerted by the flow on the bed and on the characteristics of the bed material, sediment can be transported in several different modes. The present study considers the

† Present address: IPST, GA TECH, 500 10th Street NW, Atlanta, GA 30318, USA.

mode known as bedload transport, for which the particles remain in close proximity to the bed, sliding, rolling and saltating over it. Differential transport of sediment particles gives rise to a bed topography that changes in time. One example of this is the time evolution of straight river channels in non-cohesive material. The mathematical modelling of this problem is of great theoretical interest in the area of river mechanics. The relatively simple geometry makes the study of different fundamental physical relationships between sediment transport and fluid mechanics less difficult. In the present paper emphasis is placed on explaining the mechanics of bank erosion. In order to concentrate solely on this phenomenon further simplifications are made, e.g. the bed material is assumed to be uniform in size and the suspended sediment carried by the flow and the straight channel secondary currents are neglected. Understanding the process of bank erosion in this comparatively simple case provides a key to a better understanding of more complicated problems related to bank erosion, e.g. meandering and braiding.

Theoretical models describing the motion of saltating grains under the influence of fluid flow are presented by Wiberg & Smith (1985), Anderson & Haff (1988), Sekine & Kikkawa (1992) and Sekine & Parker (1992). These models estimate the relevant physical parameters associated with bedload transport from a Lagrangian description of the trajectories of saltating grains over a bed composed of similar particles. Although the saltation models are physically the most complete available, their application in practical calculations can be very cumbersome, and so far they have been developed for beds that are inclined only slightly relative to the horizontal.

There is, however, a simpler mechanistic approach to the calculation of bedload transport. The details of motion of saltating grain are replaced by a bulk formulation based on the average grain velocity tangential to the bed surface. The effect of collision of saltating grains with the bed is replaced by a bulk dynamic coefficient of Coulomb friction. The motion of a particle placed on a laterally sloping bed is essentially determined by two forces acting on it, the drag force from the flow field and the downslope force of gravity. It can be expected that because of the lateral component of gravity the particle will not move parallel to the near-bed fluid velocity vector. The effect of transverse gravitational component is not in general linearly dependent on lateral bed slope.

In the bulk formulations implemented to date (by e.g. Glover & Florey 1951; Engelund 1974; Engelund & Fredsoe 1976; Luque & van Beek 1976; Struiksma *et al.* 1984; Parker & Andrews 1985; Ikeda 1989; Johannesson & Parker 1989), however, the assumption of small bed slope allows for simplification of the problem. These earlier formulae all include important elements of the mechanism of bedload transport. The assumptions and simplifications of the respective derivations make their applications restricted to cases where bed slope is low. For many problems of interest, this shortcoming does not necessarily impose severe limitations on the applications of the formulae. There is, however, another class of problems for which the ability to predict a vectorial bedload transport rate up to the angle of repose of the sediment is crucial. One such problem, that of bank erosion, is considered in the present paper. It was the failure of existing treatments of transverse bedload transport on side slopes to describe bank erosion that led to this analysis of bedload transport.

The present bedload formulation represents an attempt to overcome the essential drawbacks of the available linear semi-empirical formulations, so as to adequately describe bedload transport on steep side slope near the water margin. The derivation of the new bedload model is based on a formulation presented independently by Ashida & Michiue (1972) and Engelund & Fredsoe (1976). Their formulation describes

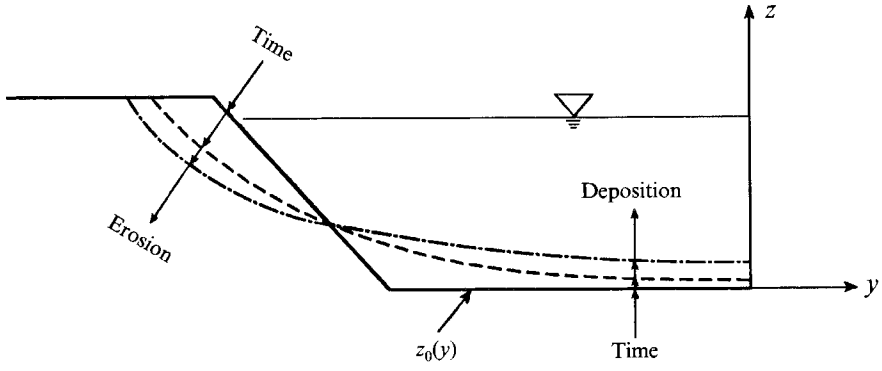

FIGURE 1. Sketch of the time development of a straight river channel; erosion of the bank, deposition around the channel centre.

the steady motion of the particle averaged over many saltations. In the present formulation the force balance equation for a particle placed on an arbitrarily sloping bed is not simplified with the consideration of low slope. The Bagnold hypothesis (1956), so far used for bedload transport on flat beds only, is herein generalized for any possible configuration. The nonlinear, fully vectorial, mechanistic formulation obtained here is thus able to cope with a far wider variety of problems in sediment transport than its predecessors. Without the new bedload model, the sediment transport process, by which straight channels evolve in time, can be simulated neither mechanistically on the entire erodible bed nor with any accuracy in time (Kovacs 1992).

The easiest way to visualize the time evolution of straight river channels is via the description of a laboratory experiment devoted to the study of channel widening through bank erosion.

In the experiments by Ikeda (1981), by Diplas (1990) and by Izumi *et al.* (1991), a long straight flume was filled with coarse material of uniform size. These experiments modelled a half cross-section of a straight channel. The channel centre was replaced with a smooth Plexiglas or painted steel wall. This configuration acted to suppress meandering tendencies by lowering the width–depth ratio (e.g. Blondeaux & Seminara 1985). The smoothness of the wall ensured that the flow field was influenced only within a very short distance from the surface, so that the wall can be considered as the axis of symmetry for a complete cross-section.

The slope of the flume and the water discharge were set at the beginning and kept constant during each run. An initial half trapezoidal cross-sectional shape was moulded into the sediment, and the flow of water was begun. At the entrance to the flume, sediment was fed/recirculated to prevent degradation of the upstream reach. The interaction of fluid and sediment caused the cross-sectional shape to widen via bank erosion, thus evolving toward a dynamic equilibrium. This equilibrium state was reached when a static equilibrium (i.e. no sediment motion) became established on the bank region, while the central bed region was characterized by non-vanishing streamwise sediment transport. The evolution toward equilibrium is summarized in figure 1.

The mathematical formulation of the time evolution of the flow field and bed topography is given by the unsteady sediment continuity equation (i.e. Exner equation) coupled with the unsteady fluid momentum equation (or a formulation yielding the local streamwise bed shear stress distribution for any given time and bed geometry).

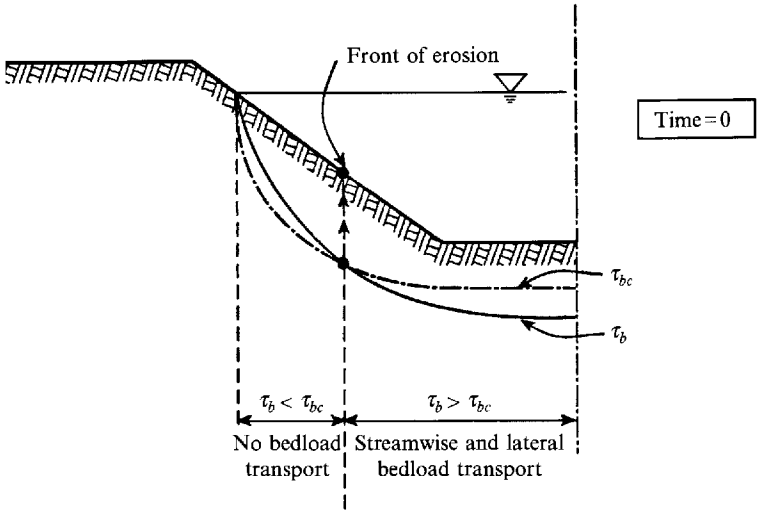

FIGURE 2. Definition of the front of erosion for an initially trapezoidal cross-section at time = 0.

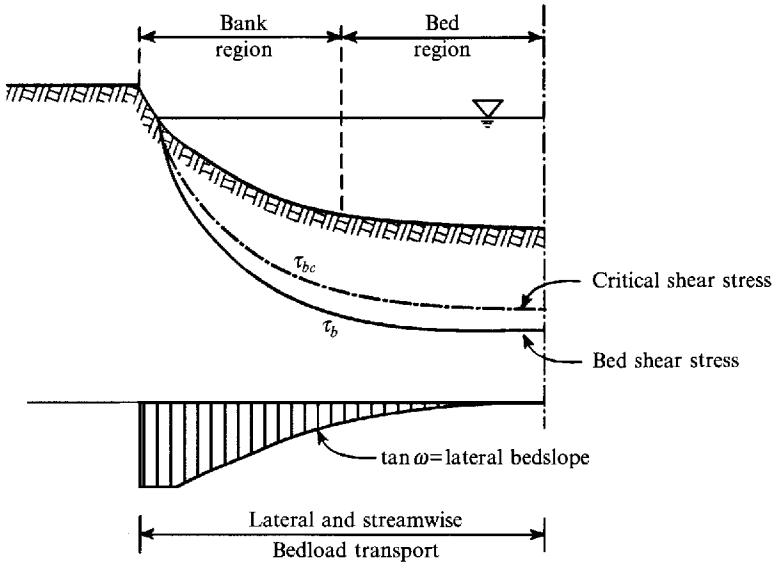

FIGURE 3. Sketch of the distribution of shear stress τ_b and lateral bedslope $\tan\omega$ along the perimeter of a straight channel cross-section, during the development of a stable profile.

One of the most important elements of the physics of the phenomenon in question is the fluid shear stress distribution on the bed, because this provides the link between the flow field and the bed geometry. The flow exerts shear stress τ_b on the mobile bed, and the bed responds by changing its shape. The change in the bed geometry takes place through the motion of individual sediment particles.

Figures 2, 3 and 4 illustrate the time history of the shear stress distribution on the bed in the case of an initially trapezoidal cross-section corresponding to the previously-described experiments. Comparing the fluid shear stress distribution τ_b to the shear stress distribution critical for sediment motion τ_{bc}, the initial cross-section can be divided into two regions, as shown in figure 2. The point on the bank which separates the two regions defines a front of erosion which begins migrating upslope, as shown on

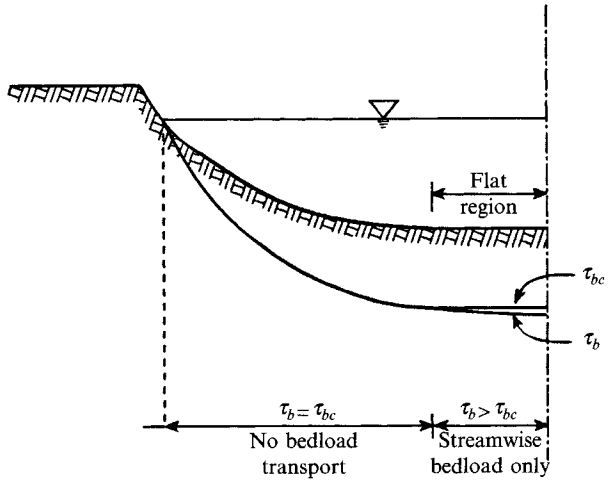

FIGURE 4. Shear stress distribution in a state of dynamic equilibrium.

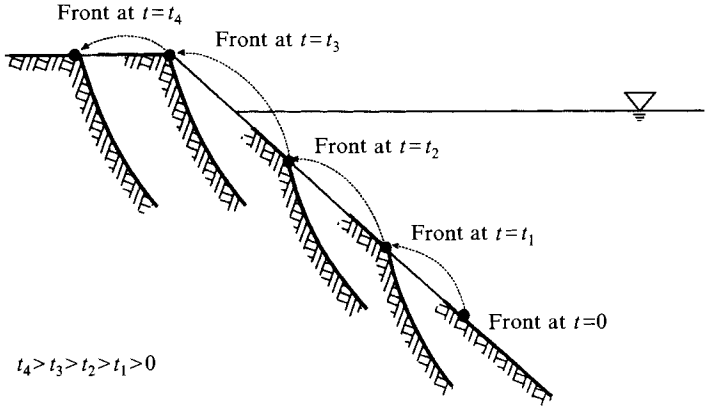

FIGURE 5. Migration of the front of erosion upslope in the case of an initially trapezoidal cross-section.

figure 5. It is always (except at the initial time) a point of discontinuity in the lateral slope and inherently separates regions of vanishing and non-vanishing lateral sediment transport. In the present study a discontinuity analysis is used to determine the migration speed of a front of erosion. The front of erosion ceases to exist (i.e. does not migrate outward any more) when dynamic equilibrium is achieved, because the dynamic equilibrium is characterized by the absence of transverse bedload, as shown in figure 4.

Early models of equilibrium channel shape in non-cohesive material, obtained by Glover & Florey (1951) and Lane, Lin & Liu (1959) use the so-called area method, which neglects the shear stress redistribution due to turbulent diffusion in the outer flow region, to compute boundary shear stress. The equilibrium state predicted by their work is characterized by vanishing bedload transport and a cross-sectional profile without a central mobile-bed region. These methods thus fail to predict equilibrium mobile-bed channels. Parker (1978*b*) recognized the importance of turbulent diffusion in this regard. Applying the closure embodied in the modified area method of Lundgren & Jonsson (1964), he obtained a bed shear stress distribution, shown on figure 4, which allows a mobile bed to coexist with an immobile bank.

A pioneering numerical simulation of this problem has recently been presented by Pizzuto (1990). He calculates the shear stress distribution on the bed from the modified area method of Lundgren & Jonsson (1964) and applied a sediment transport model which is linear in transverse bed slope. Substituting the lateral bedload relation into the Exner equation, Pizzuto (1990) obtains a one-dimensional transient diffusion equation for bed elevation. As this bedload formulation becomes invalid for angles well below the angle of repose, the widening process must be artificially initiated with a heuristic failure model at the water margin. Wiele (1992) gives a comprehensive summary of previous methods to calculate bed shear stress distribution and bank erosion in a straight channel with non-cohesive sediment. Similarly to Pizzuto (1990), Schippa (1991) and Wiele (1992) apply a bedload formulation which is linear in lateral slope, and introduce as a sediment boundary condition at the bank top the lateral flux from the collapsed sediment edge.

In the present study, the application of the new fully nonlinear vectorial bedload formulation allows the Exner equation to be classified as a transient advection–diffusion equation. At the front of erosion the Exner equation becomes a simple wave equation, and a line of weak discontinuity (i.e. a characteristic) appears in the solution. The proper form of the essential boundary condition for the sediment continuity equation is prescribed along the characteristic line of the front of erosion.

It must be emphasized that the aim of the present work is to develop a mathematical model which is physically correct (both as regards the calculation of the shear stress and lateral bedload flux), fully mechanistic (in other words there are no heuristic parts in the description of the process) and contains a minimum of empirical parameters or constants.

2. General vectorial bedload model in tensor invariant form

The aim of this section is to compute the vectorial bedload transport rate at any point of a bed formed from non-cohesive granules of uniform size. In order to do this, the Ashida–Michiue (1992) relation for a horizontal bed is generalized to a fully vectorial bedload formulation for arbitrary bed shear stress vector and an arbitrarily sloping bed, up to the angle of repose.

2.1. *Geometry*

Let $z = f(\boldsymbol{r})$ denote the vertical elevation of the bed surface; $\boldsymbol{r}$ denotes the position vector, e.g. $\boldsymbol{r} = (x, y)$ in an (x, y, z)-rectangular Cartesian coordinate system. It is assumed in the present derivation that the surface is smooth and can be locally approximated by the corresponding infinitesimal tangent plane. It is further assumed that the radius of curvature of the bed surface is much larger than the average saltation length of a particle. As a result, bed surface curvature need not be taken into account in a consideration of bedload transport.

Let $\hat{\boldsymbol{n}}$ denote the unit normal vector to the bed surface and $-\hat{\boldsymbol{k}}$ represent the unit downward vertical vector. The unit downward vertical vector $-\hat{\boldsymbol{k}}$ can be decomposed into a component normal and a component tangential to the plane of the bed. These are defined as

$$\boldsymbol{k}_n = -(\hat{\boldsymbol{k}}\cdot\hat{\boldsymbol{n}})\hat{\boldsymbol{n}}, \quad \boldsymbol{k}_t = -\hat{\boldsymbol{k}} + (\hat{\boldsymbol{k}}\cdot\hat{\boldsymbol{n}})\hat{\boldsymbol{n}}, \tag{1a, b}$$

respectively. The bed slope is then expressed by

$$\tan\beta = |\boldsymbol{k}_t|/|\boldsymbol{k}_n| \tag{2}$$

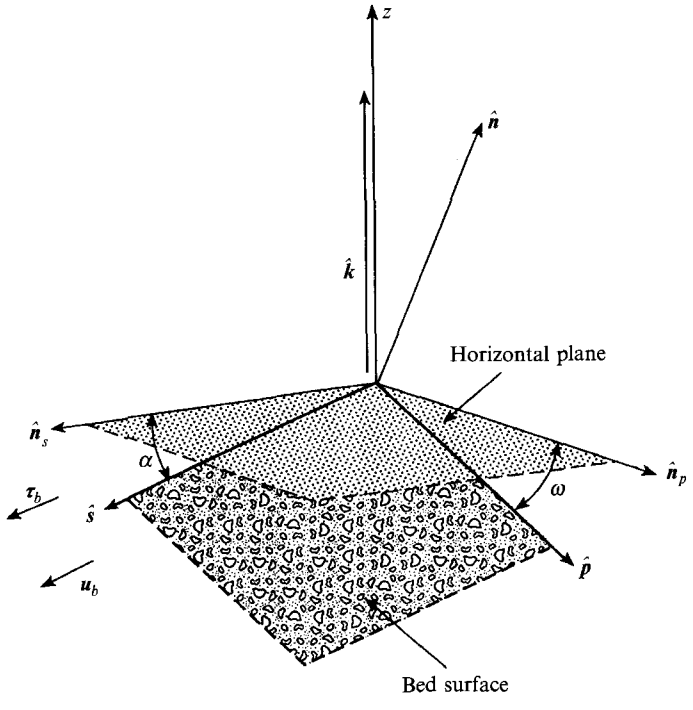

FIGURE 6. Geometry for the new bedload formulation.

where β denotes the bed slope angle.

Suppose now that fluid is flowing over the bed and exerts a shear stress $\boldsymbol{\tau}_b$ on the surface. By definition the shear stress is tangential to the bed surface, i.e. $\boldsymbol{\tau}_b \cdot \hat{\boldsymbol{n}} = 0$. The unit vector tangent to the surface in the direction of the applied fluid shear stress is defined as follows;

$$\hat{\boldsymbol{s}} = \frac{\boldsymbol{\tau}_b}{|\boldsymbol{\tau}_b|}. \tag{3}$$

The streamwise and lateral slopes of the bed $\tan\alpha$ and $\tan\omega$ can be obtained from the corresponding directional derivatives of the bed surface;

$$\tan\alpha = \hat{\boldsymbol{n}}_s \cdot \nabla z, \quad \tan\omega = \hat{\boldsymbol{n}}_p \cdot \nabla z, \tag{4a, b}$$

respectively, where

$$\hat{\boldsymbol{n}}_s = \frac{(\hat{\boldsymbol{k}} \times \hat{\boldsymbol{s}}) \times \hat{\boldsymbol{k}}}{|(\hat{\boldsymbol{k}} \times \hat{\boldsymbol{s}}) \times \hat{\boldsymbol{k}}|}; \quad \hat{\boldsymbol{n}}_p = \frac{\hat{\boldsymbol{k}} \times \hat{\boldsymbol{s}}}{|\hat{\boldsymbol{k}} \times \hat{\boldsymbol{s}}|}. \tag{5a, b}$$

Two special cases of interest are worth noting here. In the case of a bed sloping only in the streamwise direction, $\omega = 0$ and $\beta = \alpha$. In the case of a bed sloping only in the transverse direction, $\alpha = 0$ and $\beta = \omega$.

The unit tangent to the surface in the direction of the lateral slope is

$$\hat{\boldsymbol{p}} = \frac{\hat{\boldsymbol{n}}_p - \hat{\boldsymbol{k}} \tan\omega}{|\hat{\boldsymbol{n}}_p - \hat{\boldsymbol{k}} \tan\omega|}. \tag{6}$$

The bed configuration and the above defined unit vectors are shown in figure 6. Note that in general $\hat{\boldsymbol{s}}$ and $\hat{\boldsymbol{p}}$ are not orthogonal to each other.

2.2. *Stress and velocity*

It is assumed here that the flow is fully turbulent, and that there exists a fully rough turbulent inner layer near the surface of the bed. The bedload layer, an effective layer where the particles can be in motion, is located within this inner layer, extending only a few grain diameters above the bed. The representative bed shear stress $\boldsymbol{\tau}_b$ is given within the inner layer, at the top of the bedload layer. The effective near-bed flow velocity $\boldsymbol{u}_b$ (an ensemble mean fluid velocity) is assumed to be parallel to $\boldsymbol{\tau}_b$ (see e.g. Engelund & Skovgaard 1973), and is evaluated by means of the rough logarithmic law of the wall. Thus

$$\boldsymbol{u}_b = u_b \hat{\boldsymbol{s}}; \quad \boldsymbol{\tau}_b = \tau_b \hat{\boldsymbol{s}}, \tag{7a,b}$$

where

$$\frac{u_b}{u_*} \equiv a^{\frac{1}{2}} = \frac{1}{\kappa} \ln\left(30 \frac{n}{k_s}\right)\Big|_{n=m_1 D}. \tag{8}$$

In the above relation, κ denotes the Kármán constant, assumed to take a value of 0.4, $u_* = (\tau_b/\rho)^{\frac{1}{2}}$ denotes the shear velocity and ρ is the fluid density. In addition, k_s denotes the roughness height of the bed, which can in general be taken to be some multiple of grain size D; that is, $k_s = m_2 D$. In line with the simplifying assumption of Ashida & Michiue (1972), the time varying fluid velocity felt by a grain as it saltates is replaced by a constant 'effective' fluid velocity evaluated at a set distance above the bed. Here this distance is taken to be $n = m_1 D$ which defines a characteristic height above the bed in the bedload layer where the fluid drag on a moving grain is taken to act. Ashida & Michiue (1972) chose $m_1 = m_2 = 1$.

It is seen from (7) and (8) that

$$\boldsymbol{u}_b = u_b \hat{\boldsymbol{s}} = (a\tau_b/\rho)^{\frac{1}{2}} \hat{\boldsymbol{s}}, \tag{9a}$$

or rephrasing with the aid of (7),

$$\rho |\boldsymbol{u}_b| \boldsymbol{u}_b = a\boldsymbol{\tau}_b. \tag{9b}$$

2.3. *Forces*

Sediment particles can be in motion within the thin bedload layer, saltating over the plane of the bed illustrated in figure 6. Assuming that particle saltation has achieved some local statistical equilibrium, and in addition that the motion of the particle is averaged over many saltations, the particle can be considered to move with a steady mean particle velocity $\boldsymbol{v}_p$. Although $\boldsymbol{v}_p$ must be tangential to the bed surface it is not in general parallel to $\boldsymbol{u}_b$ owing to the effect of gravity acting on the grain. In the present study, the mean motion of the particle is determined by the drag force, the immersed weight of the particle and the Coulomb resistive force. The particle is taken to be spherical.

The drag force $\boldsymbol{F}_D$ which the moving fluid exerts on the particle is given as:

$$\boldsymbol{F}_D = \tfrac{1}{2}\rho c_D \pi(\tfrac{1}{2}D)^2 |\boldsymbol{u}_r| \boldsymbol{u}_r, \tag{10}$$

where $\boldsymbol{u}_r$ denotes the fluid velocity relative to the moving particle, given by

$$\boldsymbol{u}_r = \boldsymbol{u}_b - \boldsymbol{v}_p, \tag{11}$$

and c_D stands for the drag coefficient.

The immersed weight of the particle is calculated assuming that the pressure distribution in the flow can be approximated as hydrostatic. The component of the immersed weight of the particle tangential to the plane of the bed is $\boldsymbol{W}_g$, given by

$$\boldsymbol{W}_g = \rho R g \pi \tfrac{4}{3}(\tfrac{1}{2}D)^3 \boldsymbol{k}_t, \tag{12}$$

where $R = (\rho_s/\rho - 1)$ denotes the submerged specific gravity of the particle, ρ_s is the sediment density and g is the magnitude of the acceleration due to gravity.

During saltations the particles collide with the bed and lose part of their momentum. Since the motion of a particle is characterized by a velocity averaged over many saltations, the momentum loss due to collision with the bed must be represented in the bulk by a force resisting the mean motion of the particle. This force is the dynamic Coulomb resistive force $\boldsymbol{F}_c$, which can be taken to be proportional to the immersed weight of the particle normal to the bed;

$$\boldsymbol{F}_c = -\hat{\boldsymbol{t}}_{vp}\rho R g \pi \tfrac{4}{3}(\tfrac{1}{2}D)^3 |\boldsymbol{k}_n| \mu_C, \tag{13a}$$

where

$$\hat{\boldsymbol{t}}_{vp} = \frac{\boldsymbol{v}_p}{|\boldsymbol{v}_p|} \tag{13b}$$

denotes a unit vector in the direction of particle motion. The coefficient of proportionality is the dynamic Coulomb friction factor μ_C. Various numerical experiments on saltation (e.g. Sekine & Kikkawa 1992) suggest that μ_C can be approximated as a constant. This constant furthermore does not appear to differ greatly from the static Coulomb friction factor μ_s associated with incipient failure of slopes composed of granules. That is, $\tan^{-1}(\mu_C)$ provides a reasonable approximation of the angle of repose, $\tan^{-1}(\mu_s)$. It is assumed for simplicity here that μ_s is equal to μ_C.

2.4. *Force balance on a moving sediment particle*

The approximation that the particle moves with a steady mean particle velocity $\boldsymbol{v}_p$ implies that the forces acting on the particle are in equilibrium:

$$\boldsymbol{F}_D + \boldsymbol{W}_g + \boldsymbol{F}_c = 0. \tag{14}$$

From (14) it is clear that these forces represent forces in the bulk. Equation (14) reduces with the aid of (10)–(13) to the following dimensionless form;

$$\frac{1}{a}|\boldsymbol{u}_r^*|\,\boldsymbol{u}_r^* = \tau_{co}^*\left(|\boldsymbol{k}_n|\,\hat{\boldsymbol{t}}_{vp} - \frac{\boldsymbol{k}_t}{\mu_C}\right). \tag{15a}$$

Here the dimensionless velocity $\boldsymbol{u}_r^* = \boldsymbol{u}_b^* - \boldsymbol{v}_p^*$ has been formed by dividing the respective dimensioned forms $\boldsymbol{u}_r, \boldsymbol{u}_b, \boldsymbol{v}_p$ by the velocity scale $(RgD)^{\frac{1}{2}}$. The parameter τ_{co}^* is given by the relation

$$\tau_{co}^* = \frac{4}{3}\frac{\mu_C}{a c_D}. \tag{15b}$$

This parameter is in fact identical to the dimensionless Shields critical shear stress for the onset of grain motion over a horizontal bed in the Ashida–Michiue (1972) formulation, as illustrated below.

2.5. *The threshold of motion*

The particles protruding from the bed surface are the ones immediately exposed to the impelling drag of the fluid. If the fluid shear stress acting at the bed is gradually increased from zero, it can be observed that there is a critical shear stress value above which a significant number of the particles on the bed are placed in motion. This critical shear stress corresponds to the threshold of motion.

At the threshold of motion, then, the force balance on a sediment particle is satisfied

with zero particle velocity. In the case $v_p^* = 0$, the dimensionless force balance equation (15a) reduces to

$$\frac{1}{a}|u_{bc}^*|\,u_{bc}^* = \tau_{co}^*\left(|k_n|\,\hat{t}_{vp}^o - \frac{k_t}{\mu_C}\right). \tag{16a}$$

Here $\hat{t}_{vp}^o$ is a unit vector denoting the initial direction of motion

$$\hat{t}_{vp}^o = \hat{t}_{vp}|_{v_p=0} \tag{16b}$$

and u_{bc}^* indicates the critical dimensionless near-bed fluid velocity

$$u_{bc}^* = u_b^*|_{v_p=0} = u_{bc}^*\hat{s}. \tag{16c}$$

A critical bed shear stress τ_{bc} and a dimensionless critical Shields stress τ_c^*, both pertaining to the threshold of motion, can be determined as follows:

$$\tau_{bc} \equiv \tau_b|_{v_p=0}\hat{s} \equiv \tau_{bc}\hat{s}, \quad \tau_c^* = \frac{\tau_{bc}}{\rho RgD}. \tag{17a, b}$$

It is seen from (17) that the critical Shields stress is in general a vectorial quantity, possessing a direction parallel to the applied shear stress. Equations (9b) and (16a) together with (17) yield, upon reduction, the following relation for τ_c^*,

$$\left|\frac{\tau_c^*}{\tau_{co}^*}\hat{s} + \frac{k_t}{\mu_C}\right| = |k_n|. \tag{18}$$

Equation (18) brings out rather clearly the fact that at the same point on an inclined bed, the critical Shields stress for moving grains upslope is larger than that required to move grains downslope. This is because in the former case gravity counteracts the impelling shear stress, whereas in the latter case it acts to enhance it.

Several special cases are embedded in (18). The simplest is that of a horizontal bed, for which $k_t = 0$, $|k_n| = 1$. It follows that $\tau_c^* = \tau_{co}^*$ in this case, completing the identification of τ_{co}^* as the critical Shields stress on a horizontal bed.

In the case of vanishing lateral slope, i.e. $k_t \times \hat{s} = \omega = 0$, (18) reduces to

$$\tau_c^* = \tau_{co}^*\cos\beta\left(1 - \frac{\tan\beta}{\mu_C}\right). \tag{19a}$$

Recall that in this case the angle of maximum bed slope β become identical to the streamwise slope angle α. The nonlinear dependence on streamwise angle is clearly apparent from the relation. A form similar to (19a) has been derived by Luque & van Beek (1976).

In the case of vanishing streamwise slope, i.e. $k_t \cdot \hat{s} = \alpha = 0$, a similar reduction of (18) yields

$$\tau_c^* = \tau_{co}^*\cos\beta\left(1 - \frac{\tan^2\beta}{\mu_C^2}\right)^{\frac{1}{2}}, \tag{19b}$$

where β is identical with the transverse slope angle ω. This relation has been obtained previously by, for example, Lane (1953). The nonlinear dependence on transverse angle is again readily apparent.

It is of value to note that in addition to the inclination of the bed, the critical shear stress value is a function of the properties of the sediment via the parameters μ_C and τ_{co}^*.

2.6. *Velocity of a moving particle*

If the fluid shear stress exceeds the critical value, that is, $\tau^* > \tau_c^*$ at some point on the bed, the sediment particles there are set in motion. The equation of force balance (15*a*) can then be solved to obtain the dimensionless particle velocity vector

$$\boldsymbol{v}_p^* = v_p^* \hat{\boldsymbol{t}}_{vp}. \tag{20}$$

Equation (15*a*) must be solved under the constraint that $\hat{\boldsymbol{t}}_{vp}$, defined by (13*b*), is a unit vector parallel to $\boldsymbol{v}_p$, and thus $\boldsymbol{v}_p^*$. This treatment for sediment particle velocity is essentially Lagrangian in nature.

2.7. *Bagnold condition*: *bedload vector*

In order to compute the vectorial volume bedload transport rate per unit width $\boldsymbol{q}_b$, it is necessary to determine the volume of particles participating in bedload transport per unit bed area, i.e. the sediment content parameter ξ. In the analysis of bedload transport on a flat bed, Ashida & Michiue (1972) and Engelund & Fredsoe (1976) achieved this with the use of the Bagnold (1956) hypothesis.

The sediment particles moving within the confines of a definable effective bedload layer above the bed are shown in figure 7. As this thin layer contains moving sediment particles, its bulk density is greater than that of water alone, and can be taken to be equal to $\eta\rho$ where $\eta > 1$.

Consider now on the local plane of figure 7 the illustrated small volume in the form of an elementary parallelepiped with height ζ normal to the bed. Here ζ corresponds to the thickness of the bedload layer. Assuming steady motion, the force balance per unit bed area acting on this infinitesimal box can be expressed as

$$\boldsymbol{\tau}_b + \boldsymbol{w}_G = \boldsymbol{\tau}_G + \boldsymbol{\tau}_B, \tag{21a}$$

where

$$\boldsymbol{w}_G = \zeta(\eta-1)\rho g \boldsymbol{k}_t, \quad \boldsymbol{\tau}_G = \zeta(\eta-1)\rho g\, |\boldsymbol{k}_n|\, \mu_C\, \hat{\boldsymbol{t}}_{vp}. \tag{21b, c}$$

With reference to figure 7, the interpretation of the terms in (21*a*) is as follows.

The parameter $\boldsymbol{\tau}_b$ ($= \tau_b \hat{\boldsymbol{s}}$) is the impelling force of the fluid shear stress acting at the top of the bedload layer, which is assumed to be sufficiently thin compared to the depth of flow so as to allow for the neglect of momentum input to the fluid phase from gravity within it. The parameter $\boldsymbol{w}_G$ is the component of the immersed weight of the grains in the bedload layer per unit bed area acting tangential to the bed.

The forward momentum of the flow imparted to the grains via drag is transferred to the bed by means of oblique partially elastic collision, giving rise to a 'grain stress' $\boldsymbol{\tau}_G$. According to (21*c*), it is represented as a Coulomb frictional stress, with magnitude equal to the coefficient μ_C times the normal component of the submerged weight per unit area of the grains. As defined by (21*a*) and (21*c*), it always acts in opposition to the direction of motion. Finally, $\boldsymbol{\tau}_B$ is the fluid shear stress acting at the bottom of the bedload layer.

In the absence of sediment motion, $\eta = 1$, it then follows from (21*a*) that $\boldsymbol{\tau}_b = \boldsymbol{\tau}_B$. If sediment is in motion, conservation of mass within the control volume of figure 7 requires that

$$\eta\rho = \eta_s \rho_s + \eta_f \rho, \tag{22}$$

under the added constraint

$$\eta_s + \eta_f = 1. \tag{23}$$

Here η_s and η_f are the volume fractions of sediment and water, respectively, within the bedload layer. Using (22) and (23), (21*a*) can be reduced to the following dimensionless form:

$$\boldsymbol{\tau}^* + \xi^* \boldsymbol{k}_t = \mu_C\, \xi^*\, |\boldsymbol{k}_n|\, \hat{\boldsymbol{t}}_{vp} + \boldsymbol{\tau}_B^*. \tag{24}$$

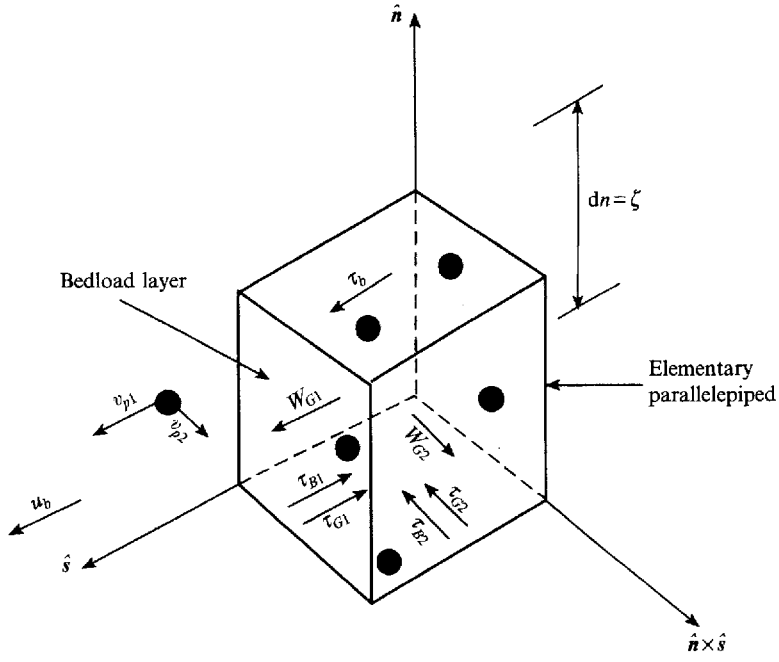

FIGURE 7. Force balance on an elementary parallelepiped; see text. Subscripts 1 and 2 refer to vector components in $\hat{s}$ and $\hat{n}\times\hat{s}$ directions, respectively, e.g. $w_G = w_{G1}\hat{s} + w_{G2}\hat{n}\times\hat{s}$.

In the above relation,

$$\boldsymbol{\tau}^* = \frac{\boldsymbol{\tau}_b}{\rho RgD} = \tau^*\hat{s}, \quad \boldsymbol{\tau}_B^* = \frac{\boldsymbol{\tau}_B}{\rho RgD}, \tag{25a, b}$$

denote the vectorial Shields stress applied to the top and bottom of the bedload layer, respectively, and

$$\xi^* = \frac{\xi}{D} \quad \text{where} \quad \xi = \zeta\eta_s. \tag{26a, b}$$

In (24), τ^*, $|\boldsymbol{k}_n|$, $\boldsymbol{k}_t$, and μ_C are prescribed parameters. The unit vector $\hat{\boldsymbol{t}}_{vp}$ is obtained from a solution of (20). Thus (24) contains a scalar and a vectorial unknown: the dimensionless volume of bedload sediment per unit bed area ξ^* and the bottom fluid Shields stress vector $\boldsymbol{\tau}_B^*$. In so far as (24) represents a relation between coplanar vectors in the plane of the bed, it provides one less constraint than needed to solve for ξ^*, and $\boldsymbol{\tau}_B^*$.

According to the Bagnold (1956) hypothesis for bedload transport over a horizontal bed, when the particles are in motion the bottom fluid Shields stress should become equal to the corresponding critical value τ_{c0}^*. It follows in the case of (24) that a corresponding condition must be placed on $\boldsymbol{\tau}_B^*$ in order to allow for solution. It is also seen that even in the general case, the Bagnold condition must be scalar in nature in order to obtain proper closure.

The simplest possible generalization to the vectorial case is the hypothesis that the streamwise component of the bottom fluid shear stress is equal to the critical value appropriate for the slope of the bed in question; that is,

$$\boldsymbol{\tau}_B^* \cdot \hat{s} = \tau_c^*, \tag{27}$$

where τ_c^* is computed from (18).

Reducing (24) with the aid of (27) the following solution is obtained for ξ^*:

$$\xi^* = \frac{\tau^* - \tau_c^*}{(\mu_C |\boldsymbol{k}_n| \hat{\boldsymbol{t}}_{vp} - \boldsymbol{k}_t) \cdot \hat{\boldsymbol{s}}}. \tag{28}$$

The above relation represents an Eulerian rather than Lagrangian formulation. It is then possible to solve for $\boldsymbol{\tau}_B^*$ as well. According to (28), the content of moving sediment in the bedload layer increases linearly with fluid shear stress acting at the bed. From (24) and (27), it is similarly seen that the component of $\boldsymbol{\tau}_B$ perpendicular to the streamwise direction, i.e. $\boldsymbol{\tau}_B \cdot (\hat{\boldsymbol{n}} \times \hat{\boldsymbol{s}})$, is determined solely by the corresponding perpendicular components of the Coulomb friction and the tangential gravity force.

Continuity can be used to represent the vectorial volume bedload transport rate of bed sediment per unit normal width $\boldsymbol{q}_b$ in the following form

$$\boldsymbol{q}_b = \xi \boldsymbol{v}_p. \tag{29}$$

This relation can be rendered dimensionless by dividing through by $((RgD)^{\frac{1}{2}} D)$, such that $\boldsymbol{q}_b^*$ is defined equal to $\boldsymbol{q}_b/((RgD)^{\frac{1}{2}} D)$. This yields the form

$$\boldsymbol{q}_b^* = \xi^* \boldsymbol{v}_p^*. \tag{30}$$

With this result the original aim of the calculation is achieved: a generalized predictor of the quantity $\boldsymbol{q}_b$ has been specified.

In the case of bedload transport over a horizontal bed, with the help of $|\boldsymbol{k}_n| = 1$, $\boldsymbol{k}_t = 0$, $\hat{\boldsymbol{s}} \equiv \hat{\boldsymbol{t}}_{vp}$ and $\tau_c^* \equiv \tau_{co}^*$ in (8), (11), (15) and (28), equation (30) reduces to

$$\boldsymbol{q}_b^* = q_b^* \hat{\boldsymbol{s}} = \frac{a^{\frac{1}{2}}}{\mu_C} (\tau^* - \tau_{co}^*)(\tau^{*\frac{1}{2}} - \tau_{co}^{*\frac{1}{2}}) \hat{\boldsymbol{s}}. \tag{31}$$

This corresponds to the Ashida–Michiue (1972) relation.

At a sufficiently high slope the magnitude of the critical Shields stress τ_c^* required to move a grain down the slope drops to zero as seen from (18). Likewise, it is seen from (28) that at the same high slope the dimensionless bedload volume content ξ^* becomes infinite. Both these conditions represent the expected singularity associated with a bed slope angle equal to that of the angle of repose, i.e. $\tan\beta = |\boldsymbol{k}_t|/|\boldsymbol{k}_n| = \mu_C$. With this in mind, it is seen that the formulation behaves consistently at the angle of repose.

2.8. *Sample calculation*

Herein similarly to the original model of Ashida & Michiue (1972), the parameters μ_C, a and τ_{co}^* must be specified in order to implement the model. The parameters μ_C and a further collapse into the single parameter $a^{\frac{1}{2}}/\mu_C$. Ashida & Michiue (1972) recommended that τ_{co}^* be selected from a standard Shields diagram (see e.g. Raudkivi 1976). They suggested the values $\mu_C = 0.50$ and $a^{\frac{1}{2}} = 8.5$, yielding a value of 17 for $a^{\frac{1}{2}}/\mu_C$. Ashida & Michiue (1972) obtained excellent agreement upon comparing their formulation to an extensive body of experimental data.

For the present sample calculation, the following somewhat modified values are used: $\mu_C = 0.84$, $a^{\frac{1}{2}} = 11.9$ (corresponding to $m_1 = 3.89$ and $m_2 = 1$ in (8)), and $\tau_{co}^* = 0.035$; these are justified in §3.4. Note that the selected value of μ_C corresponds to a dynamic friction angle $\tan^{-1}(\mu_C)$ of 40°, i.e. close to the static angle of repose of the sediment.

For the purposes of numerical experimentation, the streamwise angle of inclination α is fixed, and the lateral angle ω is allowed to change continuously from zero to the value at which τ_c^* vanishes. Two cases are considered for α. In the first case $\tan\alpha$ is chosen to be vanishing, and in the second case it is set equal to $\frac{3}{4}\mu_C$.

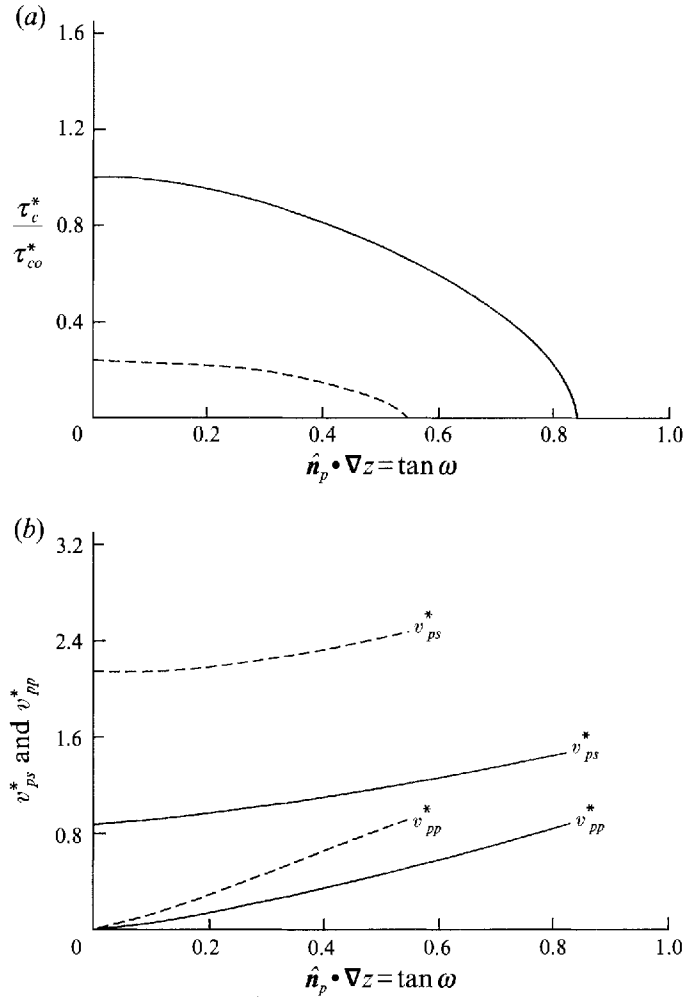

FIGURE 8(*a*,*b*). For caption see facing page.

The results of the calculations are shown in figure 8. In figure 8(*a*) the ratio of critical Shields stress on a sloping bed to that on a horizontal bed, τ_c^*/τ_{co}^*, is plotted versus $\tan\omega$. In the case $\tan\alpha = 0$, τ_c^*/τ_{co}^* is seen to vary from unity at $\tan\omega = 0$ to zero at $\tan\omega = \mu_C$. In the case $\tan\alpha = \frac{3}{4}\mu_C$, τ_c^*/τ_{co}^* takes only the value 0.21 at $\tan\omega = 0$, dropping to 0 at a value of $\tan\omega$ of 0.55. A marked increase in mobility of grains is seen as either streamwise or transverse slope is increased.

Figures 8(*b*)–8(*d*) pertain to mobile-bed conditions, with the value of Shields stress τ^* taken to be twice the critical value τ_{co}^* for a flat bed. Figure 8(*b*) shows v_{ps}^* and v_{pp}^*, figure 8(*c*) shows ξ^*, and figure 8(*d*) shows q_{bs}^* and q_{bp}^* as functions of $\tan\omega$. The subscripts s and p denote vector components in the streamwise $\hat{\boldsymbol{s}}$ and lateral $\hat{\boldsymbol{p}}$ directions, respectively, e.g. $\boldsymbol{q}_b^* = q_{bs}\hat{\boldsymbol{s}} + q_{bp}\hat{\boldsymbol{p}}$. It is evident from the plots that the model yields infinite transport rates, and thus fails for lateral angles higher than those yielding a vanishing critical Shields stress τ_c^*, for the mechanistically well-founded reason that the slope itself should, in fact, fail under such conditions.

More specific verification of the new bedload formulation is provided in terms of the prediction of straight channel evolution presented in §3.

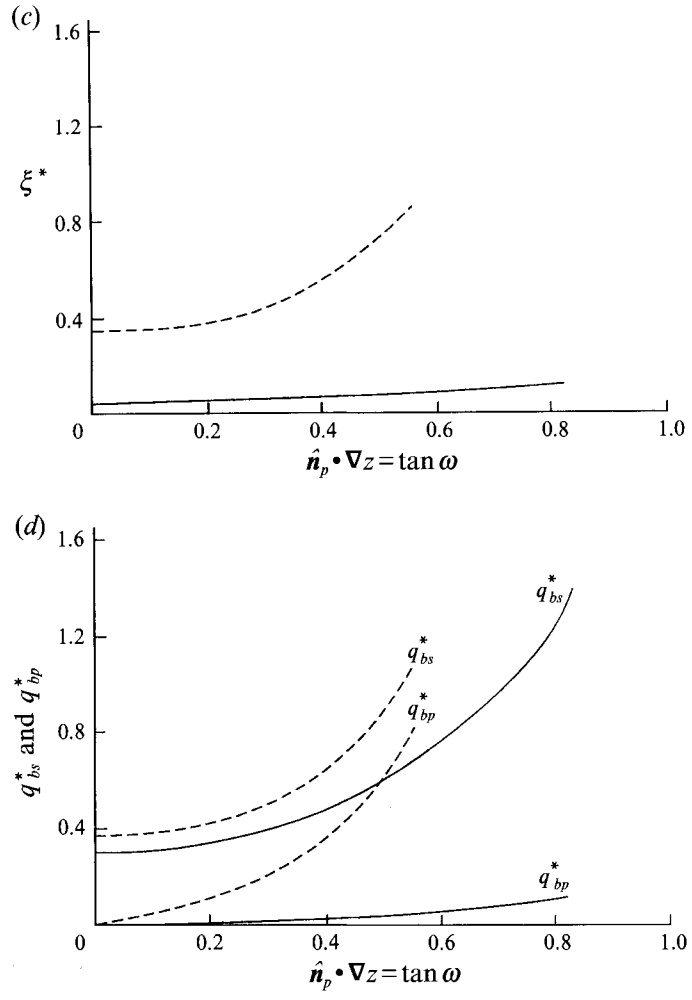

FIGURE 8. (*a*) Critical shear stress for ——, $\tan\alpha = 0$, – – –, $\tan\alpha = \frac{3}{4}\mu_C$. (*b*) Particle velocity vector $\boldsymbol{v}_p$ $(= v_{ps}\hat{\boldsymbol{s}} + v_{pp}\hat{\boldsymbol{p}})$ for ——, $\tan\alpha = 0$ and – – –, $\tan\alpha = \frac{3}{4}\mu_C$. (*c*) Sediment content parameter ξ^* for ——, $\tan\alpha = 0$; – – –, $\tan\alpha = \frac{3}{4}\mu_C$. (*d*) Bedload vector $\boldsymbol{q}_b$ $(= q_{bs}\hat{\boldsymbol{s}} + q_{bp}\hat{\boldsymbol{p}})$ for ——, $\tan\alpha = 0$; – – –, $\tan\alpha = \frac{3}{4}\mu_C$.

2.9. *Further remarks*

The new formulation still leaves considerable room for improvement. Bedload transport models of the type of Ashida & Michiue (1972) represent approximate bulk treatments averaged over many saltations. Improved results would probably be obtained through the use of a full saltation model. To date, such models have been implemented only for the cases of bedload transport on a horizontal bed (e.g. Wiberg & Smith 1985; Sekine & Kikkawa 1992), and a bed sloping mildly in the transverse direction (Sekine & Parker 1992). In principle, it should be possible to extend such saltation models to the case of high transverse slopes.

In the present analysis, the dynamic Coulomb friction factor μ_C for moving grains has been assumed to be equal to the static value μ_s. In a more complete model, μ_C would approach μ_s smoothly in the limit of vanishing motion.

Implementations of the above formulation can also be found in Kovacs (1992) and

Parker & Kovacs (1992); within which a working program in the Pascal language is provided.

3. Time development of straight self-formed channels

3.1. *Flow field evolution*

In open channels the mean turbulent flow of the viscous, incompressible fluid known as water is governed by the Reynolds and continuity equations;

$$\rho\left(\frac{\partial \boldsymbol{u}}{\partial t}+\boldsymbol{u}\cdot\nabla\boldsymbol{u}\right)=-\nabla p+\rho\boldsymbol{g}+\mu\nabla^2\boldsymbol{u}+\nabla\cdot\boldsymbol{\tau}, \tag{32}$$

$$\nabla\cdot\boldsymbol{u}=0. \tag{33}$$

Here t is the time, $\boldsymbol{u}$ is the ensemble mean part of the velocity field, p is the ensemble mean pressure, $\boldsymbol{g}$ is the acceleration due to gravity (such that $|\boldsymbol{g}|=g$), ρ is the fluid density and μ is the dynamic viscosity of the fluid. $\boldsymbol{\tau}$ is the Reynolds stress tensor, the components of which are given by

$$\tau_{ij}=-\rho\overline{u_i'u_j'}, \tag{34}$$

where u_i' is the ith component of the fluctuating part of the velocity field.

For the present analysis of the flow field a Cartesian coordinate system (x', y', z') is set up at the axis of symmetry of the straight channel such that $\boldsymbol{u}=(u, v, w)$. The streamwise (primary) velocity component u and the secondary flow components v and w are in the x'-, y'- and z'-directions, respectively, as shown in figure 9. The streamwise slope of the channel is $\tan\alpha$, where α is the angle of the x'-axis to a horizontal plane.

The origin of the secondary flow is embedded in the structure of turbulence in straight channels, as discussed by e.g. Einstein & Li (1958), Gessner & Jones (1965), Demuren & Rodi (1984), Speziale (1987, 1991), Nezu, Nakagawa & Tominaga (1985) and Tamburrino (1990). It is estimated that the magnitude of straight-channel secondary flow is approximately 1% of the mean flow. Here the details of the secondary flow itself are not treated.

It is also assumed that the term $\partial\boldsymbol{u}/\partial t$ is negligible in (32), so that the unsteadiness enters the flow field evolution only through the changing boundaries of the flow. The condition under which this quasi-steady flow approximation is valid (e.g. Kovacs 1992) is

$$q_{sed}/q_{flow}\ll 1. \tag{35}$$

Here q_{flow} stands for an average water discharge per unit width and q_{sed} denotes a characteristic volume bedload transport rate per unit width. In a typical channel studied in this paper this ratio is less than 10^{-3}. Straight channel secondary currents are taken to be negligible here, and the bed geometry and flow field are taken to be independent of x. Applying the Boussinesq (1877) eddy-viscosity concept to (32), the following momentum equation for the streamwise mean velocity can be obtained,

$$\rho g\sin\alpha+\frac{\partial}{\partial y'}\left\{(\mu+\mu_t)\frac{\partial u}{\partial y'}\right\}+\frac{\partial}{\partial z'}\left\{(\mu+\mu_t)\frac{\partial u}{\partial z'}\right\}=0. \tag{36}$$

Here $\mu_t=\mu_t(y', z')$ denotes an isotropic turbulent eddy diffusivity. The other two components of the Reynolds equation yield the condition that the pressure distribution is essentially hydrostatic, i.e. $\partial p/\partial z'=\rho g\cos\alpha$.

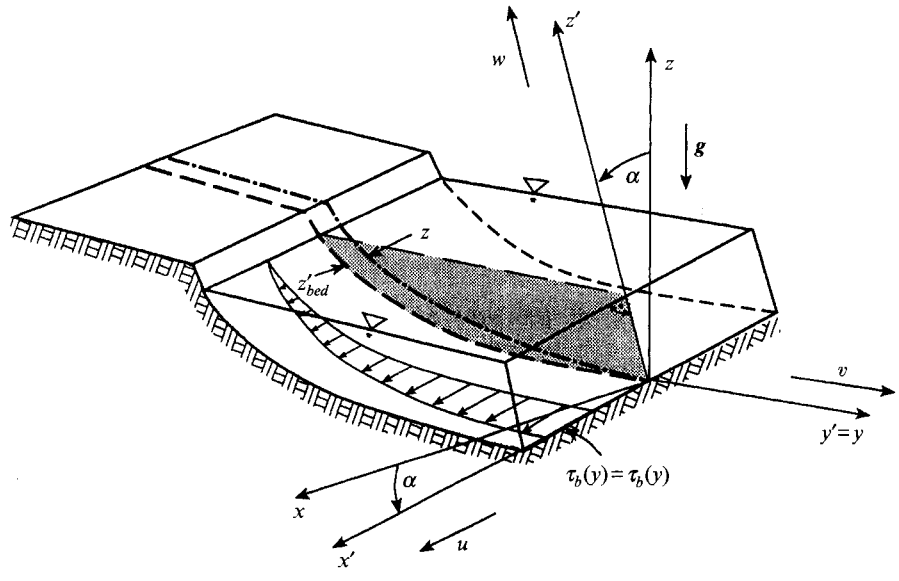

FIGURE 9. Geometry of a straight channel illustrating the connection between the (x', y', z')-coordinate system of the Reynolds equation and the (x, y, z)-coordinate system of the Exner equation.

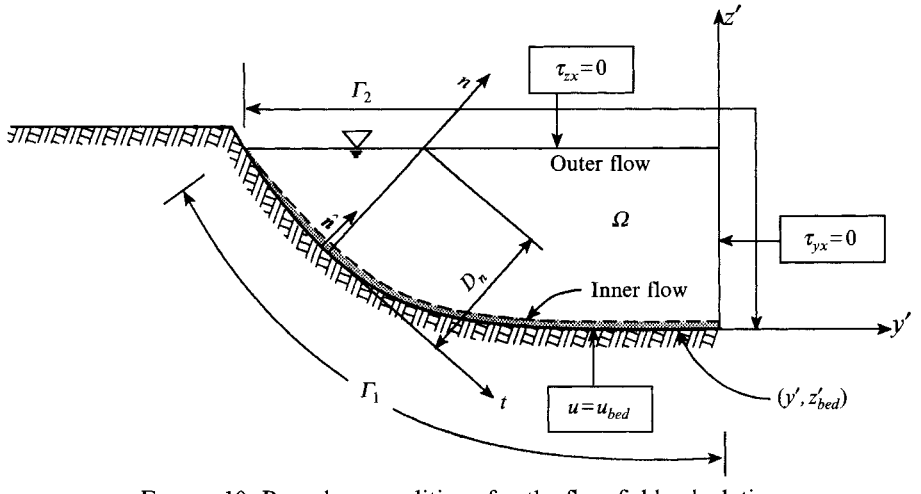

FIGURE 10. Boundary conditions for the flow-field calculation.

The boundary conditions and the flow field are illustrated in figure 10. Along the bed $z'_{bed}(y')$, denoted also by Γ_1, the essential boundary condition is prescribed

$$u = u_{bed} = 0 \quad \text{on } \Gamma_1. \tag{37}$$

Along the free surface and the axis of symmetry, denoted by Γ_2, the natural boundary condition corresponding to vanishing shear stress (τ_{yx} or τ_{zx}) is given as

$$\hat{\boldsymbol{n}} \cdot \{(\mu + \mu_t) \nabla u\} = 0 \quad \text{on } \Gamma_2. \tag{38}$$

Note that the bed shear stress, τ_b, can be calculated from the velocity gradient at the bed;

$$\tau_b = \hat{\boldsymbol{n}} \cdot \{(\mu + \mu_t) \nabla u\} = (\mu + \mu_t) \frac{\partial u}{\partial n} \quad \text{on } \Gamma_1, \tag{39}$$

where $\hat{\boldsymbol{n}}$ is the unit vector normal to the bed.

Consider now the time evolution of the flow field, so that at any time t it occupies the region $\Omega(t)$, where $\Omega(t)$ denotes the domain bounded by $\Gamma_1 U \Gamma_2$. On integration of the fluid velocity, u, over the domain, Ω, the flow discharge

$$Q = \int_{\Omega(t)} u \, \mathrm{d}y' \, \mathrm{d}z' \tag{40}$$

is obtained. Recall that the water discharge, Q, is held constant during the experiments. The mass conservation expressed by (40) provides an integral condition to determine the location of the free-surface boundary (i.e. the centre water depth, $H_c(t)$, in the channel).

3.2. *Evolution of bed topography*

3.2.1. *Governing equation: Exner equation*

Conservation of sediment is described by the Exner equation, which has the following form in an (x, y, z) Cartesian coordinate system:

$$\frac{\partial z}{\partial t} + \frac{1}{1-\lambda_p} \nabla \cdot \boldsymbol{q}_{sed} = \frac{\partial z}{\partial t} + \frac{1}{1-\lambda_p} \left(\frac{\partial q_x}{\partial x} + \frac{\partial q_y}{\partial y} \right) = 0, \tag{41}$$

where z $(= z(x, y, t))$ is the time-dependent vertical elevation of the bed surface above a horizontal reference plane, x and y are horizontal coordinates of a bed point, $\boldsymbol{q}_{sed}$ is the bedload vector of sediment flux with Cartesian components q_x and q_y in the x and y directions, respectively, and λ_p is the porosity of the bed sediment. Equation (41) is valid in the absence of suspended sediment since, as noted in § 1, it is assumed here that the sediment is coarse enough to preclude its suspension. The effect of suspended sediment has been investigated (e.g. Parker 1978*a*). A more complex case with heterogeneous bed material is discussed by e.g. Ikeda, Parker & Kimura (1988).

For the present analysis the (x, y, z) coordinate system, shown in figure 9, is defined such that the y'-axis used in the description of the flow field coincides with the y-axis of the x, y, z system (i.e. $y' \equiv y$ and $z'_{bed} = z \cdot \cos\alpha$). Thus, in this system α remains the angle of the streamwise slope and ω $(= \omega(y, t))$ denotes the angle of the lateral slope, as shown in figures 9 and 11.

Figure 11 also illustrates how the general vectorial bedload transport model is related to the bedload vector employed in (41). Thus

$$\boldsymbol{q}_{sed} = (\boldsymbol{q}_b \cdot \hat{\boldsymbol{n}}_s)\hat{\boldsymbol{i}} + (\boldsymbol{q}_b \cdot \hat{\boldsymbol{n}}_p)\hat{\boldsymbol{j}} \tag{42a}$$

or

$$q_x = q_{bs} \cos\alpha, \quad q_y = q_{bp} \cos\omega. \tag{42b}$$

Here $\boldsymbol{q}_b$ denotes the bedload flux vector tangent to the bed surface with components q_{bs} and q_{bp} in the streamwise and lateral directions, respectively.

For the straight channel shown in figure 9 the assumption of uniformity in the streamwise direction x simplifies (41) as well. The partial differential equation to solve for the time evolution of the cross-sectional geometry of a straight channel $(z = z(y, t))$ is thus:

$$\frac{\partial z}{\partial t} + \frac{1}{1-\lambda_p} \frac{\partial q_y}{\partial y} = 0. \tag{43}$$

In the following two sections the Exner equation is analysed with the help of the new bedload formulation and the integral form of the sediment conservation equation.

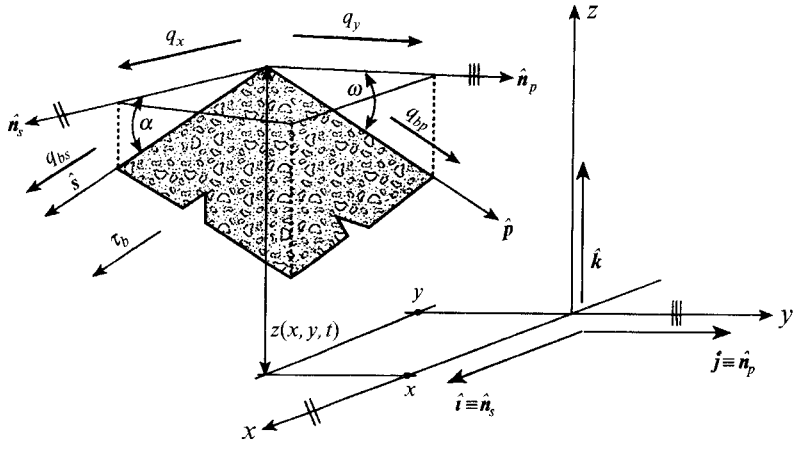

FIGURE 11. The components of the bedload vector in the Exner equation (i.e. (41)) as calculated with the general vectorial bedload model of §2.

3.2.2. *Hyperbolic nature of the Exner equation*

The sediment continuity equation must be classified as a partial differential equation in order to obtain information to prescribe the correct boundary conditions. With the help of the new generalized vectorial bedload formulation derived in §2, (43) becomes

$$\frac{\partial z}{\partial t} = -\frac{\partial z}{\partial y}\frac{f_1 f_2 \dfrac{\partial(\tau_b - \tau_{bc})}{\partial y} + (\tau_b - \tau_{bc})\dfrac{\partial(f_1 f_2)}{\partial y}}{1-\lambda_p} - \frac{\partial^2 z}{\partial y^2}\frac{f_1 f_2(\tau_b - \tau_{bc})}{1-\lambda_p}. \tag{44}$$

Here $f_1 > 0$ and $f_2 > 0$ are known functions which are obtained in a straightforward way through the application of the new fully nonlinear bedload formulation. That is

$$f_1 = \frac{1}{Rg\rho(\mu_C |\boldsymbol{k}_n| \hat{\boldsymbol{t}}_{vp} - \boldsymbol{k}_t)\cdot\hat{\boldsymbol{s}}}, \quad f_2 = \frac{\tau^*_{co}|\boldsymbol{v}_p||\boldsymbol{k}_n|^2}{\mu_C\left(\tau^*_{co}|\boldsymbol{k}_n| + \dfrac{1}{a}|\boldsymbol{u}^*_r||\boldsymbol{v}^*_p|\right)}. \tag{45a,b}$$

Equation (44) is a time dependent advection–diffusion (i.e. a hyperbolic–parabolic type) equation for the bed elevation in the cross-section. At the point where the bed shear stress τ_b is equal to the critical value for sediment motion τ_{bc} the bed elevation is governed by a nonlinear first-order hyperbolic equation of the form

$$\frac{\partial z}{\partial t} = -\frac{\partial z}{\partial y}\frac{f_1 f_2}{1-\lambda_p}\frac{\partial(\tau_b - \tau_{bc})}{\partial y} \quad \text{at} \quad y = y_F. \tag{46}$$

Since (44) becomes a nonlinear simple wave equation (i.e. (46)) at one point in the domain, it allows propagation of weak discontinuities there along a characteristic. It should also be remembered that (44) holds only on the side of the characteristic line where the particles are in motion (i.e. $\tau_b > \tau_{bc}$). On the other side of the characteristic the particles are at rest (i.e. $\tau_b < \tau_{bc}$) and the bedload flux is equal to zero; i.e. $q_y \equiv 0$ and consequently $\partial z/\partial t \equiv 0$. The point separating these two regions defines the front of erosion. In (46), y_F denotes the y-coordinate of the erosional front. Near the front of erosion the sediment transport process becomes advection dominated, while near the channel centre it is dominated by diffusion.

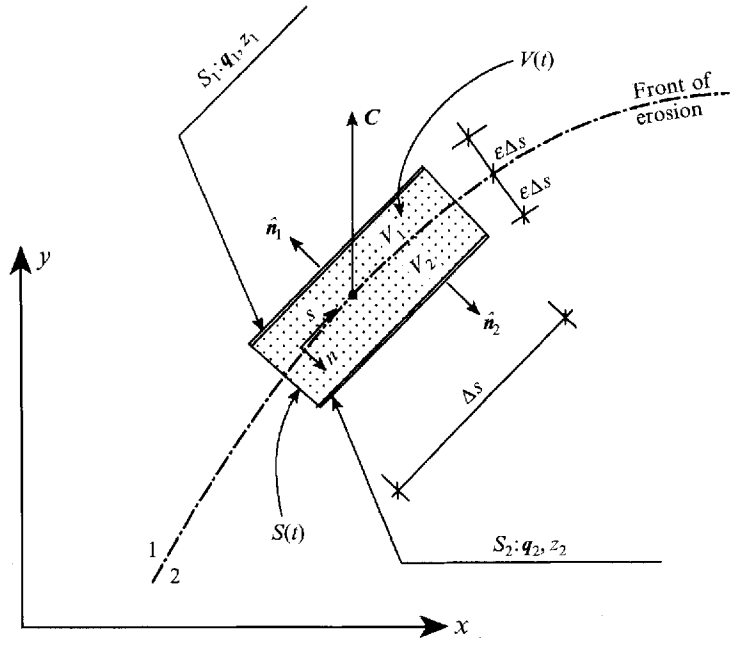

FIGURE 12. Moving control volume at the front of erosion.

The mathematical theory developed for nonlinear wave equations in fluid dynamics can be applied to analyse the present problem. More details on this subject can be found (e.g. Thompson 1971; Whitham 1974).

3.2.3. *Erosional front velocity*

The motion of sediment across the front must satisfy the sediment continuity equation. In case of discontinuities in flow properties the integral forms of the conservation equations are utilized. For an arbitrary moving control volume the integral form of the sediment conservation equation is

$$\frac{\mathrm{d}}{\mathrm{d}t}\int_{V(t)} z\,\mathrm{d}V = -\frac{1}{1-\lambda_p}\int_{S(t)} \boldsymbol{q}_{sed}\cdot\hat{\boldsymbol{n}}\,\mathrm{d}S + \int_{S(t)} \boldsymbol{b}\cdot\hat{\boldsymbol{n}} z\,\mathrm{d}S. \tag{47}$$

Here, $V(t)$ and $S(t)$ are the moving control volume and control surface, respectively, $\hat{\boldsymbol{n}}$ is an outward unit normal from the control surface and $\boldsymbol{b}$ is the local boundary velocity with which the control surface moves.

In the left half a straight river channel, shown in figure 5, along the characteristic of the front of erosion the discontinuity in lateral slope (i.e. $\tan\omega = \partial z/\partial y$) propagates in the negative y-direction with velocity c_y. To the left of the front of erosion the lateral slope is equal to its initial value and on the right it is larger than the initial value owing to the transverse motion of the sediment particles.

To apply the discontinuity analysis for erosional fronts in general, the moving control volume shown in figure 12 is taken to enclose a portion of the front of erosion. This control volume moves with the local front velocity $\boldsymbol{c}$. In figure 12, side 1 is the side where the sediment flux is zero and side 2 is the side where the sediment flux is non-zero. The control volume is arbitrarily thin, and its surfaces parallel to the front are small. Fitting a local (n, s)-coordinate system to the erosional front, the side dimension of the control volume is Δs and the half thickness of the control volume

is $\epsilon\Delta s$, where ϵ is an arbitrarily small number. The control volume set up this way is used to provide a local jump condition for the front of erosion in the normal derivative of z.

In applying the integral balance statement (47) to the control volume shown in figure 12, the contribution of the edges ($\epsilon\Delta s$) to the surface integrals can be neglected. Taking $\boldsymbol{q}_1$ and $\boldsymbol{q}_2$ to be the bedload fluxes and z_1 and z_2 to be the bed elevations on the two sides of the control volume, i.e. on S_1 and S_2, respectively, (47) can be written as

$$\frac{\mathrm{d}}{\mathrm{d}t}\int_{V_1+V_2} z\,\mathrm{d}V = \int_{S_1}\left(-\frac{\boldsymbol{q}_1\cdot\hat{\boldsymbol{n}}_1}{1-\lambda_p}+z_1\boldsymbol{c}\cdot\hat{\boldsymbol{n}}_1\right)\mathrm{d}S+\int_{S_2}\left(-\frac{\boldsymbol{q}_2\cdot\hat{\boldsymbol{n}}_2}{1-\lambda_p}+z_2\boldsymbol{c}\cdot\hat{\boldsymbol{n}}_2\right)\mathrm{d}S. \tag{48}$$

The following form of (48) holds for a moving control volume as it sweeps through the unchanged initial bed configuration z_o with velocity $\boldsymbol{c}$:

$$\frac{\mathrm{d}}{\mathrm{d}t}\int_{V_1+V_2} z_o\,\mathrm{d}V = \int_{S_1} z_{o1}\boldsymbol{c}\cdot\hat{\boldsymbol{n}}_1\,\mathrm{d}S+\int_{S_2} z_{o2}\boldsymbol{c}\cdot\hat{\boldsymbol{n}}_2\,\mathrm{d}S. \tag{49}$$

Here (49) expresses the rate of change of volume in the control volume owing to the motion of the control volume alone.

Power series expansions around the erosional front yield

$$z = z_o = z_F+\left.\frac{\partial z}{\partial n}\right|_1 n+\ldots \quad \text{in } V_1, \tag{50a}$$

$$z = z_F+\left.\frac{\partial z}{\partial n}\right|_2 n+\ldots \quad \text{in } V_2, \tag{50b}$$

$$z_o = z_F+\left.\frac{\partial z}{\partial n}\right|_1 n+\ldots \quad \text{in } V_2, \tag{50c}$$

$$z_1 = z_{o1} = z_F+\left.\frac{\partial z}{\partial n}\right|_1 (-\epsilon\Delta s)+\ldots \quad \text{on } S_1, \tag{50d}$$

$$z_2 = z_F+\left.\frac{\partial z}{\partial n}\right|_2 \epsilon\Delta s+\ldots \quad \text{on } S_2, \tag{50e}$$

$$z_{o2} = z_F+\left.\frac{\partial z}{\partial n}\right|_1 \epsilon\Delta s+\ldots \quad \text{on } S_2, \tag{50f}$$

$$\boldsymbol{q}_2\cdot\hat{\boldsymbol{n}}_2 = \left.\frac{\partial(\boldsymbol{q}_{sed}\cdot\hat{\boldsymbol{n}}_2)}{\partial n}\right|_2 \epsilon\Delta s+\ldots \quad \text{on } S_2. \tag{50g}$$

Note that for erosional fronts $\boldsymbol{q}_1$ is always equal to zero, as the bedload flux vanishes at the front of erosion. In (50), z_F denotes the bed elevation at the front of erosion (i.e. at $y = y_F$ for straight channels).

First (50) is substituted into (48) and (49), then (49) is subtracted from (48). Neglecting the volume integrals as they tend to zero, the jump condition for the front of erosion is obtained in the limit as the size of the control volume approaches zero (i.e. $\Delta s\to 0$),

$$\boldsymbol{c}\cdot\hat{\boldsymbol{n}}_2 = \frac{1}{1-\lambda_p}\frac{\left.\dfrac{\partial(\boldsymbol{q}_{sed}\cdot\hat{\boldsymbol{n}}_2)}{\partial n}\right|_2}{\left.\dfrac{\partial z}{\partial n}\right|_2-\left.\dfrac{\partial z}{\partial n}\right|_1}. \tag{51}$$

For the case of the front of erosion as it pertains to the time evolution of straight river channels (51) simplifies to the following migration celerity of the erosional front,

$$\boldsymbol{c}\cdot\hat{\boldsymbol{j}} = c_y = \frac{\mathrm{d}y_F}{\mathrm{d}t} = \frac{1}{1-\lambda_p}\frac{\left.\frac{\partial q_y}{\partial y}\right|_2}{\left.\frac{\partial z}{\partial y}\right|_2 - \left.\frac{\partial z}{\partial y}\right|_1}. \tag{52}$$

The path of the front of erosion (i.e. $y_F = y_F(t)$) defines both the characteristic of and the boundary for the sediment continuity equation (43). Equations (51) and (52) are of theoretical value. In general, neither the derivative of the sediment flux nor the lateral bed slope on side 2 are known without the numerical solution of (43). They nevertheless serve to clearly delineate how the front of erosion propagates bankward.

3.2.4. *Initial and boundary conditions*

To solve equation (43) both initial and boundary conditions must be prescribed. The initial condition at $t = 0$ is,

$$z = z(y, t = 0) = z_0(y), \tag{53}$$

which is here taken to be the initial half trapezoidal cross-sectional profile shown in figure 2. The essential boundary condition is prescribed at the front of erosion. Noting that at this point the bed elevation is equal to the initial value, the essential boundary condition is,

$$z = z_o(y) \quad \text{at} \quad y = y_F(t). \tag{54}$$

At the axis of symmetry the natural boundary condition is given as,

$$\frac{\partial z}{\partial y} = q_y = 0 \quad \text{at} \quad y = 0. \tag{55}$$

3.3. *Numerical prediction*

For turbulent flows of the type considered here, it is more convenient to replace the true boundary condition (37) by an effective wall/bed boundary condition (see e.g. Cebeci & Bradshaw 1988; Speziale 1991) given by the logarithmic rough law of the wall which is assumed to be valid in the inner layer at some distance from the wall. Thus, the 'bed' boundary condition for (36) can be specified as

$$u_{bed} = \frac{u_*}{\kappa}\ln\left(30\frac{n}{k_s}\right)\Big|_{n=n_{match}}. \tag{56}$$

Here k_s ($= 2.5D$) is the roughness height and n is a local coordinate measured upward normal from the bed. n_{match} is arbitrarily set equal to $0.01D_n$, where D_n is the total flow depth normal to the bed. Figure 10 shows the local (n, t)-coordinate system attached to the wetted perimeter $z_{bed}(y)$, denoted also by Γ_1. Boundary conditions similar to that of (56) are applied by e.g. Rodi & Scheuerer (1983) for a smooth wall, and Maron *et al.* (1991) for a rough wall.

For equation (36) the distribution of μ_t over the flow field is approximated by a simple algebraic closure

$$\mu_t = (\rho\tau_b)^{\frac{1}{2}}\kappa n\left(1-\frac{n}{D_n}\right), \tag{57}$$

as it is well known that μ_t has a nearly parabolic distribution with depth in wide open

channel flow. The derivation of this closure model (see e.g. Henderson 1966) is based on Prandtl's mixing length concept. Equation (57) is valid in the outer flow region (i.e. outer layer). Rodi (1980) and more recently an ASCE Task Committee (1988) discuss several other turbulence models applied in free-surface flow problems.

Equation (36) together with (57) and (56) provide the velocity distribution in the outer layer. From the outer flow solution a near-bed shear stress distribution is obtained by (39). The bed shear stress distribution is now extrapolated from this near-bed shear stress distribution on application of the condition

$$\int_{\Gamma_1} \tau_b \, \mathrm{d}\Gamma = \rho g A \sin \alpha, \tag{58}$$

where A denotes the wetted area of the cross-section. The procedure described above does not resolve the flow structure at the wall in the inner layer, but rather predicts the bed shear stress distribution from the outer flow solution. Nevertheless, it correctly simulates the redistribution of shear stress due to turbulent diffusion in the outer flow region (Parker 1978*b*).

At the beginning of computation the turbulent eddy viscosity model based on (56) cannot be applied, as the n-lines orthogonal to the bed (see figure 10) cross each other inside the flow field. In this case the normal depth method

$$\tau_b = \rho g D_n \sin \alpha \tag{59}$$

(in combination with a temporarily fixed free-surface boundary) is used as an approximate means to calculate the bed shear stress distribution until such time as the cross-sectional geometry becomes smooth enough to allow for application of (56). The time interval in question here is very short.

Grains on the dry bank adjacent to the water's edge mostly roll and slide into the water under the effect of gravity. Strictly speaking, q_y in (43) cannot be calculated from the bedload formulation used here at a point that is not submerged. The bank collapse, illustrated in figures 1 and 5, however, requires a continuous delivery of sediment from the dry bank to the water margin as long as the channel continues to widen. It is assumed here that the motion of the particles above the water surface is similar to that under the water surface on a slope near the angle of repose. It is also assumed that the lateral slope of the dry bank is identical to that at the water margin. Particles on the dry bank are mobilized with the application of a small shear stress there. The magnitude of this shear stress is chosen just so that the lateral angle of the bank above the water margin coincides with that immediately below. This way, the new bedload relation can be used to describe bank failure in a quantitatively accurate way.

The dynamic equilibrium state is reached asymptotically when the lateral bedload vanishes everywhere in the cross-section. For practical purposes the numerical calculation can be terminated when the lateral bedload becomes so small that further changes in cross-sectional shape are negligible.

The numerical discretization of (36) and (43), presented in Kovacs (1992), applies the finite-element method, which provides a flexible discretization in space and the variable-step trapezoid rule, which incorporates the change in timescale. Kovacs (1992) also describes a numerical technique to track the migration of the front of erosion.

3.4. *Example: Ikeda's run* 17 *and parameter sensitivity:* $a^{\frac{1}{2}}$, μ_C *and* τ_{co}^*

In this section the mathematical model developed to simulate the time development of a straight self-formed channel is tested against experimental results. The experiment of choice is Ikeda's (1981) Run 17, because it is regarded as a representative case and

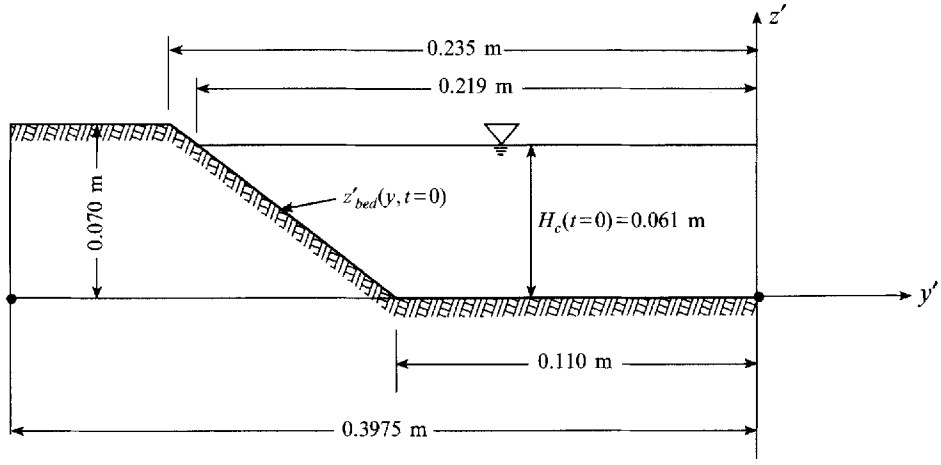

FIGURE 13. Initial bed profile and water depth of Ikeda's (1981) Run 17, corresponding to the initial conditions for the numerical experiment.

S [−]	D [m]	ρ [kg m^{-3}]	g [m s^{-2}]	R [−]	λ_p [−]	k_s [m]	μ [kg m^{-1} s^{-1}]
0.00215	0.0013	1000.0	10.0	1.65	0.35	0.0032	0.001

TABLE 1. Parameters used in the numerical calculation to stimulate Ikeda's (1981) Run 17.

therefore presented in detail by Ikeda (1981). Run 17 was also used by Pizzuto (1990) to verify his mathematical model.

The circumstances and conditions of Ikeda's experiments have been explained in § 1. Run 17 was performed in a flume with a length of 15 m and a width of 50 cm. The data measured at a cross-section located 11 m downstream of the flume inlet are compared against the results of the present numerical experiment.

The initial half trapezoidal cross-section, $z'_{bed}(y, t = 0)$, and the initial water depth in the centre, $H_c(t = 0)$, are illustrated in figure 13. For numerical computation the following parameters must be prescribed: channel slope S $(= \tan\alpha)$, median grain diameter D, water density ρ, acceleration due to gravity g, submerged specific gravity of the sediment $R = \rho_s/\rho - 1$ where ρ_s denotes sediment density, bed porosity λ_p, roughness height k_s, dynamic viscosity of water μ. The values of these parameters are listed in table 1.

There are three important parameters in sediment transport problems the values of which are widely argued in the literature. The first one is $a^{\frac{1}{2}}$, i.e. the ratio of the shear velocity to the representative fluid velocity in the bedload layer. The second one is the critical Shield stress τ^*_{co} for the onset of particle motion on horizontal bed. The third parameter is the dynamic Coulomb friction factor μ_C, the value of which is close to that of the static Coulomb friction factor. In the present case the dynamic Coulomb friction factor is approximated with the static Coulomb friction factor (see e.g. Sekine & Parker 1992), the tangent of the angle of repose. Different researchers apply different values for these parameters, e.g. Engelund & Fredsoe (1976) suggest that μ_C is approximately equal to $\tan 27° = 0.51$ and τ^*_{co} is between 0.028 and 0.056. Ikeda (1982) uses the values of $\tan 40°$ and $\tan 45°$ for the Coulomb friction factor, and calculates τ^*_{co} as a function of particle Reynolds number. Recently, Wiberg & Smith (1987) presented a thorough analysis on the calculation of the critical shear stress. They summarize the results of

Case	$a^{\frac{1}{2}}$	μ_C	τ^*_{co}	$a^{\frac{1}{2}}/\mu_C$
A	11.90	0.70	0.035	17.00
→B	11.90	0.84	0.035	14.17
C	8.953	0.70	0.035	12.79
D	8.400	0.84	0.035	10.00
E	11.23	0.80	0.035	12.79
F	11.90	0.70	0.040	17.00
G	8.400	0.84	0.030	10.00

TABLE 2. Parameters for the numerical experiments used to simulate Ikeda's (1981) Run 17.

	Case	H_c/H_{co}	B/B_o	$\tau(y=0)/\tau_{co}$	q_x/q_{xo}	Q [m^3 s^{-1}]
Run	17	0.66	1.34	—	—	0.00413
	A	0.72	1.45	1.312	0.0748	0.00403
	→B	0.74	1.36	1.350	0.1084	0.00400
	C	0.73	1.43	1.332	0.0847	0.00403
	D	0.76	1.32	1.373	0.1201	0.00395
	E	0.74	1.37	1.349	0.1033	0.00397
	F	0.79	1.29	1.253	0.0583	0.00402
	G	0.69	1.53	1.474	0.1473	0.00397

TABLE 3. Water surface width and water depth simulating Ikeda's Run 17 with different parameters. The comparison is at time = 12 h.

previous investigators to determine the value of the critical Shield stress for a flat bed as well as the value of the angle of repose for different problems. Pizzuto (1990), in his simulation of Ikeda's (1981) Run 17, finds that the best agreement with the experimental results is obtained with the application of a value of 0.65 for μ_C and a value of 0.03 for τ^*_{co}.

The developed numerical code (see Kovacs 1992) provides an excellent opportunity to investigate the effect of these parameters on the cross-sectional geometry characterizing the dynamic equilibrium state of a straight self-formed channel.

To analyse how sensitive the solution is to change in the above mentioned parameters, the simulation of Ikeda's Run 17 is repeated for different sets of parameters. A summary of the numerical experiments is given in table 2.

In the case of Run 17 Ikeda carried out measurements for a total run time of 12 h, by which time a state near dynamic equilibrium had been reached.

Table 3 shows the water surface width and the water depth at the axis of symmetry obtained at time = 12 h for all the cases described in table 2. It can be seen that the best agreement with the experimental results is obtained in Case B. This justifies why the set of parameters employed in Case B is chosen to demonstrate the characteristics of the general vectorial model in the sample calculation of §2.8.

Analysing the results of the numerical experiments, the effects of the parameters can be summarized as follows. A decrease in $a^{\frac{1}{2}}$ causes a slight increase in depth and a slight decrease in width. The result of a decrease in μ_C is a slight decrease in depth and a comparatively larger increase in width, which can be attributed to the fact that the angle of repose has become smaller. The effect of a decrease in τ^*_{co} is that the depth decreases and the width increases by a commensurate amount.

In the rest of this section the results of the computations are detailed for Case B. Figure 14 illustrates the computed time evolution of the cross-sectional geometry, and

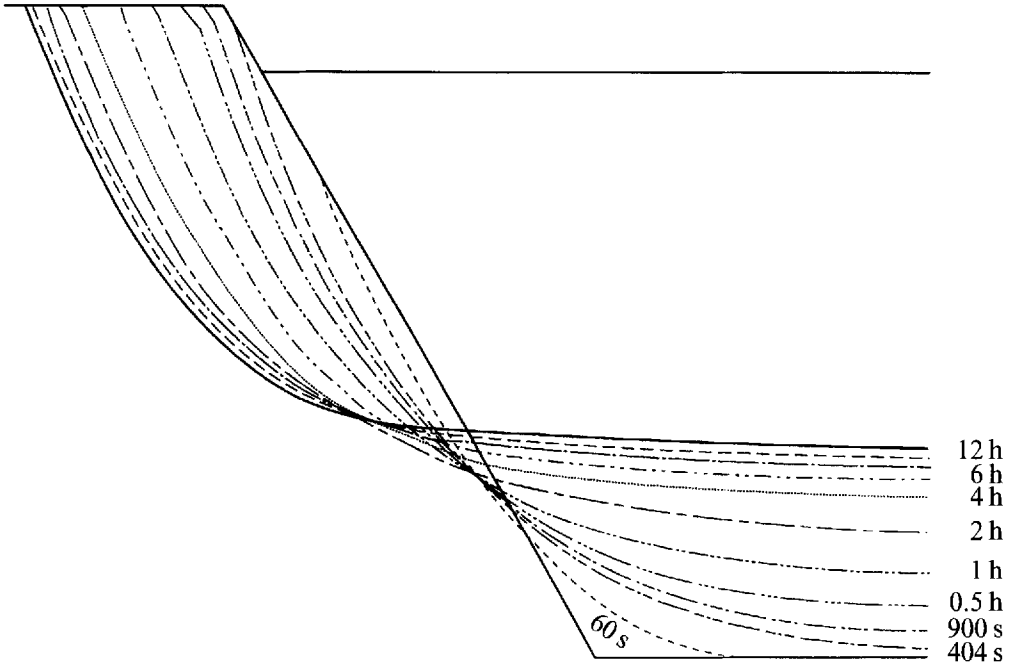

FIGURE 14. Time evolution of straight channel cross-section. The simulation is of Ikeda's (1981) Run 17.

figure 15 compares the non-dimensional cross-sections at various times from Ikeda's experiment with those of the present computation. On figure 16 the computed time evolution of non-dimensional water surface width ($B(t)/B(t=0)$) and non-dimensional centre depth ($H_c(t)/H_c(t=0)$) are compared against the observed evolution.

One of the cross-sections of figure 14, i.e. the one at $t = 404$ s, is of some interest. By $t = 404$ s the bed geometry had become smooth enough to allow for switching from the normal depth method, i.e. (59) to the full turbulent eddy diffusivity model for the computation of bed shear stress. After $t = 404$ s, then, it is possible to calculate the discharge and adjust the level of the water surface. In Ikeda's experiment the discharge is 4130 $cm^3\ s^{-1}$, while the computation keeps the discharge constant at 4000 $cm^3\ s^{-1}$ for $t > 404$ s. Fortunately, the small discharge difference and the very short time required to obtain a sufficiently smooth cross-section for implementation of the full turbulence model have negligible effect on the result of the numerical model.

The comparisons on figure 15 illustrate good agreement between the measurements and the computation. It can be seen that the Plexiglas wall of Ikeda's flume is the cause of some discrepancy. The Plexiglas wall retards the motion of the fluid and sediment, resulting in a locally steeper lateral bed slope. Another feature of interest is the longitudinal ridges evident in the experimental profiles of figure 15, especially near the end of the run. These are apparently due to weak straight channel secondary currents, which cannot be reproduced by the present flow model.

Figure 16 presents the time evolution of computed non-dimensional water surface width. Compared to the experimental results, it takes a slightly lower value for most of the calculation. The predicted final non-dimensional water surface width is, however, almost identical to that of the experiment. This situation is reversed for the non-dimensional centre depth shown also in figure 16, which is over-predicted during the entire calculation. The explanation of this difference is in the value of the roughness

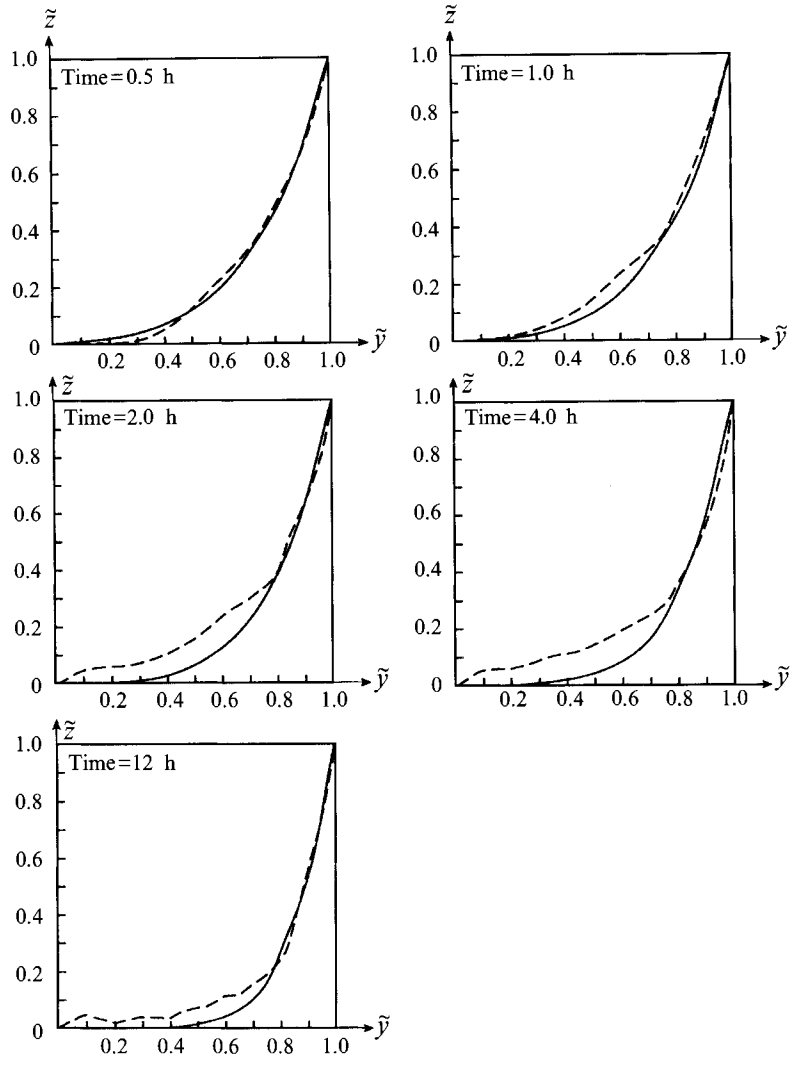

FIGURE 15. Non-dimensional cross-sections; comparison between ——, the present calculation and – – –, Ikeda's Run 17.

height. During the calculation, the roughness height k_s is held constant. An analysis of the data indicated, however, that during the physical experiment roughness height (as back-calculated from the measured flow and a relation for bed resistance) significantly decreased, even though the sediment was uniform in size. As a result of this decreased roughness height hydraulic resistance tended to decrease somewhat in time so that the straight channel in Ikeda's experiment carried the same discharge at somewhat smaller water depth. The cause of the decrease of roughness height during the experiment is not known.

Figure 17 illustrates the time variation of non-dimensional shear stress at the channel centre and the non-dimensional streamwise bedload integrated over the wetted perimeter. The non-dimensional shear stress $(\tau^*(t)/\tau^*_{co})$ at the axis of symmetry decreases from its initial value of 1.74 to a final value of 1.35 at $t = 12$ h. The non-dimensional streamwise bedload of the cross-section $(q_x(t)/q_x(t = 0))$ also decreases from 1.0 to 0.11 by the end of the calculation.

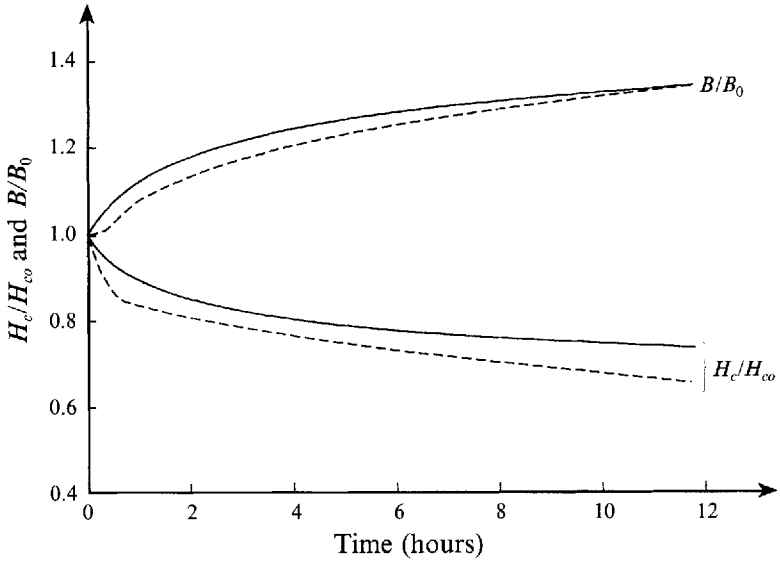

FIGURE 16. Non-dimensional water surface width and non-dimensional centre depth; Comparison between ——, the present calculation and – –, Ikeda's Run 17.

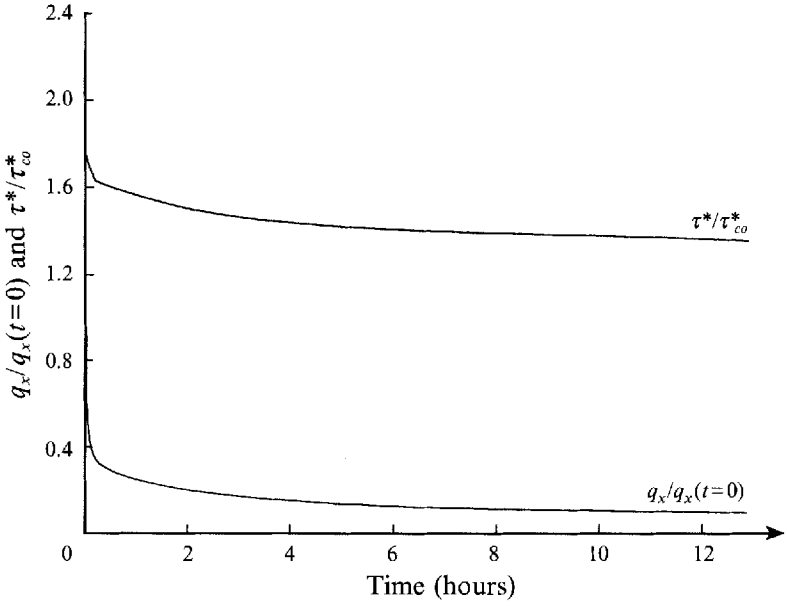

FIGURE 17. Non-dimensional shear stress in the channel centre and non-dimensional streamwise bedload transported on the half cross-section.

The computation is terminated at $t = 12$ h in correspondence to the experiment. By this time the maximum value of the lateral bedload transport rate has decreased by three orders of magnitude from its initial value. At the same time, as can be seen in figure 15, the cross-section has developed a nearly flat centre bed region. As further noticeable changes in the geometry of the cross-section cannot be expected, it can be concluded that the final dynamic equilibrium profile has essentially been reached.

4. Conclusions

The derivation of a vectorial bedload transport relation for non-cohesive sediment that is fully nonlinear in bed slope is presented. The new relation represents a straightforward generalization of the Ashida–Michiue (1972) relation, to which it reduces in the case of bedload transport over a horizontal bed. The new model contains two innovative features. It behaves as a continuous single-valued function of slope angle up to the angle of repose. In particular, the model predicts infinite transport rates on slopes so high that the critical Shields stress is reduced to zero. This is to be expected, in so far as vanishing critical Shields stress on a sloping bed corresponds to the condition of incipient slope failure. In addition, the model correctly predicts bedload transport at low Shields stress on high slopes as evidenced by its application in the numerical prediction of straight channel evolution. The new fully nonlinear and vectorial bedload formulation can be applied everywhere along the wetted perimeter of the cross-section, allowing for an entirely mechanistic calculation.

The results of the simulation of Ikeda's Run 17 compare well with the measurements. This means that the computation is time accurate, i.e. the timescale of the mathematical model, which is dictated by the bedload relation, agrees well with that observed in the experiment. The final cross-sectional profile obtained is characterized by a flat bed region near the centre of the channel, where a non-vanishing streamwise bedload is maintained. This flat region is smoothly connected to the adjacent curving bank. Along the bank the angle of the lateral slope increases up to a value close to the angle of repose. The applied simple algebraic turbulent closure model in the present numerical prediction has proved to be successful at simulating the bed shear stress distribution necessary in order to ultimately achieve a final dynamic equilibrium state.

The mechanism describing bank erosion is closely related to that describing the migration of the front of erosion. After its formation on the slope of the bank, the front of erosion moves upslope rapidly until it reaches the water's edge, and then the top of the adjacent dry bank. From then on its migrates outward, and asymptotically ceases to exist as the lateral bedload vanishes over the cross-section. The path of the front of erosion as well as the evolution of the channel can be determined by the simultaneous solution of two differential equations, those of fluid momentum conservation and the sediment continuity. In the present model at the front of erosion an essential boundary condition for the Exner equation is prescribed. This is the consequence of the application of the new bedload formulation and the correct classification of the Exner equation.

This research was supported by the National Science Foundation (grant no. CTS 891598), the Legislative Commission for Minnesota Resources and the Minnesota Supercomputer Center.

REFERENCES

ANDERSON, R. S. & HAFF, P. K. 1988 Simulation of Eolian saltation. *Science* **241**, 820–823.

ASCE TASK COMMITTEE ON TURBULENCE MODELS IN HYDRAULIC COMPUTATIONS 1988 Turbulence Modeling of Surface Water Flow and Transport: Parts I–IV. *J. Hydraul. Engng ASCE* **114**, 970–1073.

ASHIDA, K. & MICHIUE, M. 1972 Study on hydraulic resistance and bedload transport rate in alluvial streams. *JSCE Tokyo* **206**, 59–69.

BAGNOLD, R. A. 1956 The flow of cohesionless grains in fluids. *Proc. R. Soc. Lond.* A**249**, 964.

BLONDEAUX, P. & SEMINARA, G. 1985 A unified bar-bend theory of river meanders. *J. Fluid Mech.* **157**, 449–470.

BOUSSINESQ, J. 1877 Theorie de l'ecoulement tourbillant. *Mem. Pre. par. div. Sav.* 23, Paris.

CEBECI, T. & BRADSHAW, P. 1988 *Physical and Computational Aspects of Convective Heat Transfer.* Springer.

DEMUREN, A. O. & RODI, W. 1984 Calculation of turbulence-driven secondary motion in non-circular ducts. *J. Fluid Mech.* **140**, 189–222.

DIPLAS, P. 1990 Characteristics of self-formed straight channels. *J. Hydraul. Engng ASCE* **116**, 707–728.

EINSTEIN, H. A. & LI, H. 1958 Secondary currents in straight channels. *Trans. Am. Geophys. Union* **39** (6), 1085–1088.

ENGELUND, F. 1974 Flow and bed topography in channel bends. *J. Hydraul. Div. ASCE* (HY **11**), 1631–1648.

ENGELUND, F. & FREDSOE, J. 1976 A sediment transport model for straight alluvial channels. *Nordic Hydrol.* **7**, 293–306.

ENGELUND, F. & SKOVGAARD, O. 1973 On the origin of meandering and braiding in alluvial streams. *J. Fluid Mech.* **57**, 289–302.

GESSNER, F. B. & JONES, J. B. 1965 On some aspects of fully-developed turbulent flow in rectangular channels. *J. Fluid Mech.* **23**, 689–713.

GLOVER, R. E. & FLOREY, Q. L. 1951 Stable channel profiles. *US Bureau Reclamation, Washington, DC Hydrol. Lab. Rep.* 325.

HENDERSON, F. M. 1966 *Open Channel Flow.* Macmillan.

IKEDA, S. 1981 Self-formed straight channels in sandy beds. *J. Hydraul. Div. ASCE* **107** (4), 389–406.

IKEDA, S. 1982 Incipient motion of sand particles on side slopes. *J. Hydraul. Div. ASCE* **108** (1), 95–114.

IKEDA, S. 1989 Sediment transport and sorting at bends. *Am. Geophys. Union, Water Resources Monograph* **12**, 103–125.

IKEDA, S., PARKER, G. & KIMURA, Y. 1988 Stable width and depth of straight gravel rivers with heterogeneous bed materials. *Water Resources Res.* **24**, 713–722.

IZUMI, N., KOVACS, A., PARKER, G. & LUTHE, D. P. 1991 Experimental and theoretical studies of bank erosion in rivers and its prevention by low-cost means. *SAFHL Project Rep.* 320.

JOHANNESSON, H. & PARKER, G. 1989 Linear theory of river meanders. *Am. Geophys. Union, Water Resources Monograph* **12**, 181–213.

KOVACS, A. 1992 Time evolution of straight self-formed channels in non-cohesive material. PhD thesis, University of Minnesota.

LANE, E. W. 1953 Progress report on studies on the design of stable channels of the Bureau of Reclamation. *Proc. Am. Soc. Civil. Engrs* **79**, 246–261.

LANE, E. W., LIN, P. N. & LIU, H. K. 1959 The most efficient stable channel for completely clean water in non-cohesive material. *Colorado State Univ. Rep.* CER 59 HKL 5.

LUNDGREN, H. & JONSSON, I. G. 1964 Shear and velocity distribution shallow channels. *J. Hydraul. Div. ASCE* **90**, 1–21.

LUQUE, R. F. & VAN BEEK, R. 1976 Erosion and transport of bedload sediment. *J. Hydraul. Res.* **14**, 127–144.

MARON, D. M., YACOUB, N., BRAUNER, N. & NAOT, D. 1991 Hydrodynamic mechanisms in the horizontal slug pattern. *Intl. J. Multiphase Flow* **17**, 227–245.

NEZU, I., NAKAGAWA, H. & TOMINAGA, A. 1985 Secondary currents in a straight channel flow and the relation to its aspect ratio. *Turbulent Shear Flows* 4 (ed. L. J. S. Bradbury, F. Durst, B. E. Launder, F. W. Schmidt & J. H. Whitelaw), pp. 246–260. Springer.

PARKER, G. 1978*a* Self-formed rivers with stable banks and mobile bed. Part 1. The sand-silt river. *J. Fluid Mech.* **89**, 109–125.

PARKER, G. 1978*b* Self-formed rivers with stable banks and mobile bed. Part 2. The gravel river. *J. Fluid Mech.* **89**, 127–146.

PARKER, G. & ANDREWS, E. D. 1985 Sorting of bedload sediment by flow in meander bends. *Water Resources Res.* **21**, 1361–1373.

PARKER, G. & KOVACS, A. 1992 MYNORCA: A Pascal program for implementing the Kovacs–Parker vectorial bedload transport on arbitrarily sloping bed. *Tech. Mem. M*-233, *St Anthony Falls Hydr. Lab., Univ. of Minn.*

PIZZUTO, J. E. 1990 Numerical simulation of gravel bed widening. *Water Resources Res.* **26**, 1971–1980.

RAUDKIVI, A. J. 1976 *Loose Boundary Hydraulics*, 2nd edn. Pergamon.

RODI, W. 1980 Turbulence models and their applications in hydraulics. State-of-the-art paper. IAHR, Delft, The Netherlands.

RODI, W. & SCHEUERER, G. 1983 Calculation of curved shear layers with two-equation turbulence models. *Phys. Fluids* **26**, 1422–1436.

SCHIPPA, L. 1991 Model of cross-section evolution in straight alluvial channel. *Intl. Symp. on the Transport of Suspended Sediment and its Mathematical Modeling. Florence (Italy), Sept. 2–5, 1991.*

SEKINE, M. & KIKKAWA, H. 1992 Mechanics of saltating grains. II. *J. Hydraul. Engng ASCE* **118**, 536–558.

SEKINE, M. & PARKER, G. 1992 Bedload transport on a transverse slope. I. *J. Hydraul. Engng ASCE* **118**, 513–535.

STRUIKSMA, N., OLESEN, K. W., FOLKSTRA, C. & DE VRIEND, H. I. 1984 Bed deformation in curved alluvial channels. *J. Hydraul. Res.* **23**, 57–79.

SPEZIALE, C. G. 1987 On nonlinear K-l and K-ϵ models of turbulence. *J. Fluid Mech.* **178**, 459–475.

SPEZIALE, C. G. 1991 Analytical methods for the development of Reynolds-stress closures in turbulence. *Ann. Rev. Fluid Mech.* **23**, 107–57.

THOMPSON, P. A. 1971 *Compressible Fluid Dynamics.* McGraw-Hill.

TAMBURRINO, A. 1990 Flow characteristics in the moving bed flume. MSc thesis. University of Minnesota.

WHITHAM, G. B. 1974 *Linear and Nonlinear Waves.* John Wiley.

WIBERG, P. L. & SMITH, J. D. 1985 A theoretical model for saltating grains in water. *J. Geophys. Res.* **90**, 7341–7354.

WIBERG, P. L. & SMITH, J. D. 1987 Calculations of the critical shear stress for motion of uniform and heterogeneous sediments. *Water Resources Res.* **23**, 1471–1480.

WIELE, S. M. 1992 A computational investigation of bank erosion and midchannel bar formation in gravel-bed rivers. PhD thesis, University of Minnesota.